

DUDLEY KNOX LIBRARY
NATIONAL GRADUATE SCHOOL
MONTEREY CA 93943-5101

Approved for public release: distribution is unlimited.

Laser Anemometry and Viscous Computation
of the Flow Through an
Annular Turbine Cascade

by

Joseph D. Spitz
Lieutenant Commander, United States Navy
B.S., University of Rochester, 1982

Submitted in partial fulfillment
of the requirements for the degree of

MASTER OF SCIENCE IN AERONAUTICAL ENGINEERING

from the

NAVAL POSTGRADUATE SCHOOL
March 1994

REPORT DOCUMENTATION PAGE

1a Report Security Classification: Unclassified		1b Restrictive Markings	
2a Security Classification Authority		3 Distribution/Availability of Report	
2b Declassification/Downgrading Schedule		Approved for public release; distribution is unlimited.	
4 Performing Organization Report Number(s)		5 Monitoring Organization Report Number(s)	
6a Name of Performing Organization Naval Postgraduate School	6b Office Symbol (if applicable) AA	7a Name of Monitoring Organization Naval Postgraduate School	
6c Address (city, state, and ZIP code) Monterey CA 93943-5000		7b Address (city, state, and ZIP code) Monterey CA 93943-5000	
8a Name of Funding/Sponsoring Organization Naval Air Warfare Center	6b Office Symbol (if applicable) PE-31	9 Procurement Instrument Identification Number	
Address (city, state, and ZIP code) Trenton NJ 08628-0176		10 Source of Funding Numbers	
		Program Element No	Project No
		Task No	Work Unit Accession No
11 Title (include security classification) LASER ANEMOMETRY AND VISCOUS COMPUTATION OF THE FLOW THROUGH AN ANNULAR TURBINE CASCADE (UNCLASSIFIED)			
12 Personal Author(s) Spitz, Joseph D.			
13a Type of Report Master's Thesis	13b Time Covered From To	14 Date of Report (year, month, day) March 1994	15 Page Count 85
16 Supplementary Notation The views expressed in this thesis are those of the author and do not reflect the official policy or position of the Department of Defense or the U.S. Government.			
17 Cosati Codes		18 Subject Terms (continue on reverse if necessary and identify by block number)	
Field	Group	Subgroup	
		RVC3D, TCGRID, Numerical Simulation, Turbine Cascade, Laser-Doppler Velocimetry	
19 Abstract (continue on reverse if necessary and identify by block number)			
<p>An annular turbine cascade, designed for laser-Doppler velocimetry , was further modified to provide additional laser and pressure probe access. The purpose of the research was to devise laser anemometry measurement techniques in a confined annulus and improve the ability to compare numerical predictions with experimental results. Flowfield computations were completed using a viscous flow solver, with the numerical exit plane coincident with experimental measurement location. A data reduction program was written to transfer non-dimensional numerical output to the experimental coordinate system for comparison of total pressure ratio, Mach number and flow angle. Endwall two-dimensional laser measurements were obtained through a 1.0922 millimeter hole to a depth of approximately three millimeters.</p>			
20 Distribution/Availability of Abstract <input checked="" type="checkbox"/> unclassified/unlimited <input type="checkbox"/> same as report <input type="checkbox"/> DTIC users		21 Abstract Security Classification Unclassified	
22a Name of Responsible Individual Dr. Garth V. Hobson		22b Telephone (include Area Code) (408) 656-2888	22c Office Symbol CODE 31

ABSTRACT

An annular turbine cascade, designed for laser-Doppler velocimetry , was further modified to provide additional laser and pressure probe access. The purpose of the research was to devise laser anemometry measurement techniques in a confined annulus and improve the ability to compare numerical predictions with experimental results. Flowfield computations were completed using a viscous flow solver, with the numerical exit plane coincident with experimental measurement location. A data reduction program was written to transfer non-dimensional numerical output to the experimental coordinate system for comparison of total pressure ratio, Mach number and flow angle. Endwall two-dimensional laser measurements were obtained through a 1.0922 millimeter hole to a depth of approximately three millimeters.

Thesis
566858
C.I

TABLE OF CONTENTS

I.	INTRODUCTION	1
II.	EXPERIMENTAL SETUP	3
A.	TEST FACILITY	3
B.	ANNULAR TURBINE CASCADE	4
1.	GENERAL DESCRIPTION	4
2.	PRESSURE MEASUREMENT MODIFICATIONS	7
3.	LDV MODIFICATIONS	8
C.	PRESSURE PROBE	9
D.	LASER-DOPPLER VELOCIMETER	10
E.	EXPERIMENTAL PROCEDURE	11
1.	PROBE CALIBRATION	11
2.	PRESSURE PROBE MEASUREMENTS	13
3.	LDV ALIGNMENT	14
4.	ENDWALL MEASUREMENTS	15
III.	COMPUTATIONAL FLUID DYNAMICS	16
A.	GRID GENERATION	16
B.	COMPUTATIONAL SCHEME	17
IV.	RESULTS AND DISCUSSION	19
A.	PRESSURE PROBE	19

B. LASER MEASUREMENTS 23

C. NUMERICAL RESULTS 28

D. COMPARISON 32

V. CONCLUSIONS AND RECOMMENDATIONS 40

APPENDIX A. DRAWINGS 44

APPENDIX B. COBRA PROBE CALIBRATION 52

APPENDIX C. GRID GENERATION 62

APPENDIX D. RVC3D CODE INPUT 65

APPENDIX E. RVC3D DATA REDUCTION 67

LIST OF REFERENCES 73

INITIAL DISTRIBUTION LIST 74

LIST OF FIGURES

Figure 1.	Supply Pipe Schematic	4
Figure 2.	Annular Turbine Cascade Cutaway	5
Figure 3.	Blade Geometry	6
Figure 4.	Wake Positioning System	6
Figure 5.	Pressure Measurement Changes	7
Figure 6.	LDV Access Modifications	8
Figure 7.	Endwall Measurement Technique	9
Figure 8.	LDV Wiring Schematic	10
Figure 9.	Yaw Probe Calibration Equipment	12
Figure 10.	Endwall LDV Alignment Technique	14
Figure 11.	CFD Solution Comparison, 50% Span	18
Figure 12.	Pt/P0 Repeatability, 50% Span	21
Figure 13.	Pt/P0 Repeatability, Radial	21
Figure 14.	Angle Repeatability, 90% Span	22
Figure 15.	Angle Repeatability, Radial	22
Figure 16.	Single Component LDV Endwall Velocity	24
Figure 17.	Single Component LDV Turbulence	24
Figure 18.	Two Component LDV Endwall Velocity	26
Figure 19.	Two Component LDV Flow Angle	26
Figure 20.	Two Component LDV Turbulence, V-theta	27
Figure 21.	Two Component LDV Turbulence, V-z	27
Figure 22.	RVC3D Blade Pressure Ratio Plot	29
Figure 23.	PLOT3D Blade Pressure Coefficient Plot	30

Figure 24.	PLOT3D Exit Plane Mach Contour Plot	31
Figure 25.	Total Pressure Ratio Comparison, 25% . . .	34
Figure 26.	Total Pressure Ratio Comparison, 50% . . .	34
Figure 27.	Total Pressure Ratio Comparison, 75% . . .	35
Figure 28.	Total Pressure Ratio Comparison, 90% . . .	35
Figure 29.	Mach Number Comparison, 25%	36
Figure 30.	Mach Number Comparison, 50%	36
Figure 31.	Mach Number Comparison, 75%	37
Figure 32.	Mach Number Comparison, 90%	37
Figure 33.	Flow Angle Comparison, 25%	38
Figure 34.	Flow Angle Comparison, 50%	38
Figure 35.	Flow Angle Comparison, 75%	39
Figure 36.	Flow Angle Comparison, 90%	39
Figure A1.	Adjustable Pressure Probe Holder	44
Figure A2.	ATC Mounting Flange Modification	45
Figure A3.	Outer Ring Modifications	46
Figure A4.	Outer Ring Modification, Section A	47
Figure A5.	Outer Ring Modification, Section B	48
Figure A6.	Outer Ring Modification, Section C	49
Figure A7.	Plexiglas Window	50
Figure A8.	Alignment and Endwall Measurement Blank . .	51
Figure B1.	Cobra Probe Calibration Coefficients . . .	54
Figure B2.	Cobra Probe Calibration Data Plot	55
Figure B3.	Probe Validation	56
Figure C1.	Grid Geometry On Inner Hub Surface	63
Figure C2.	Grid Geometry, 3-D Perspective	64

Figure D1. RVC3D Residuals	66
--------------------------------------	----

ACKNOWLEDGEMENTS

This work could not have occurred without the personal attention of a number of talented professionals. I thank Dr. Garth Hobson for his motivation, guidance and friendship. His ability to share knowledge and develop student interest in his instruction is a gift. Professor Raymond Shreeve has always had the time to listen and I have enjoyed his enthusiasm.

Don Harvey's ability to take my vision from paper to metal has been a pleasure to behold. Rick Still and Thad Best have been more helpful than they will ever know. I count myself lucky to have had the opportunity to work with them.

My greatest thanks go to my family. Nothing that I have accomplished here has come without the incredible support and love of my partner, Deb, and my two sons, Joseph and Derrick.

I. INTRODUCTION

The non-intrusive measurement of secondary flows in annular turbines can provide insight into the design and performance of turbomachinery. Turbine stage efficiency can be improved with more precise understanding of the flow mechanics and the ability to numerically predict the response to blade redesign without manufacturing and testing.

Goldman and Seasholtz [Refs. 1-3] have conducted continuing research in the field of laser-Doppler velocimetry (LDV) measurement and numerical prediction in an annular turbine cascade. Their efforts have concentrated on obtaining comparisons ahead, in, and downstream of the blade passage. In order to obtain their results, an extensive optical system with correction for curved surfaces has been developed. To obtain two-dimensional velocity, they have measured one component and then rotated the optics to resolve the second component.

This report presents the results of laser-Doppler velocimetry techniques and three-hole pressure probe measurements in the wake of a high turning turbine nozzle. Only radial fiber-optic probe traverses were performed. Circumferential surveys were obtained by manually rotating the annular cascade blade row upstream of the measuring location. Pressure measurements were compared to numerical results

obtained using a three-dimensional viscous computer program. Laser-velocimetry techniques using two-component fiber-optic equipment were developed for the small annulus cascade including two-dimensional measurements of the endwall flow through a small access hole in the outer casing.

II. EXPERIMENTAL SETUP

A. TEST FACILITY

Airflow for the annular turbine cascade experiment was provided by a VA-312 Allis-Chalmers 12 stage axial-flow compressor housed in the Naval Postgraduate School Turbopropulsion Laboratory. The compressor was operated at 12,000 rpm at various discharge pressures. This air supply was also used to generate up to Mach 0.795 through a 107.95 mm (4.25 in) diameter nozzle for calibration of a three-hole pressure probe.

Upstream air pressure was metered through the use of two dump valves and one cutoff valve prior to a plenum chamber. Air from the plenum was directed to the test section through flow straighteners in a 254 millimeter (10 in) steel pipe as shown in Figure 1. Flow stagnation pressure was measured upstream at two locations. One combination probe was connected to a mercury manometer board located near the dump valve controls. This pressure-setting probe also provided a digital readout of flow stagnation temperature. The second probe, and the static ports in the air supply pipe, were connected to a Scanivalve for automated pressure acquisition.

LDV seed material, atomized-glycerin particles, was introduced through an eight millimeter (5/16 in) diameter

copper pipe as shown in Figure 1. Seed atomization was accomplished using laboratory compressed air with a commercial TSI, Inc., Six-Jet Atomizer. Laser traverse table buffet from the exiting flow was eliminated with a prefabricated aluminum cone (Figure 1). Flow characteristics were examined with the cone on and off, using pressure measurements and dye injection from the two chord inner hub static ports.

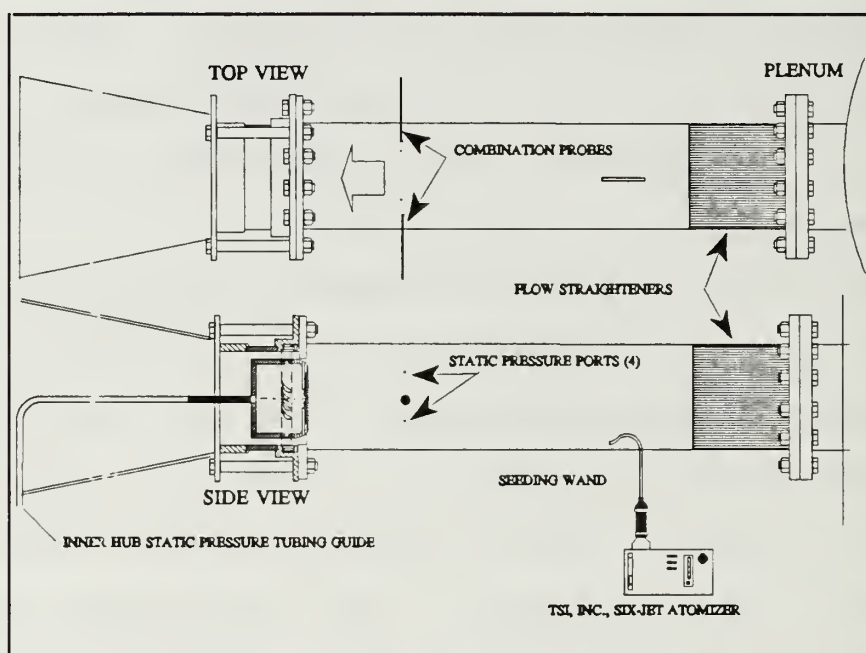


Figure 1. Supply Pipe Schematic

B. ANNULAR TURBINE CASCADE

1. GENERAL DESCRIPTION

The Annular Turbine Cascade (ATC) was developed to provide a small-scale device for flow experiment and computation on a transonic turbine stator. Thomas [Ref. 4] developed the basic apparatus. Figure 2 shows a cutaway view

of the construction of the ATC with a radial view of the blade passage just upstream of the test section. Figure 3 shows the blade geometry on a section perpendicular to the radial plane and Figure 4 shows an end view with the wake positioning capability. The inner hub radius was 98.81 mm (3.89 in) with constant blade geometry to the outer radius of 116.46 mm (4.585 in). The stator row had 31 blades with a midspan spacing of 21.77 mm (0.857 in). Reference 4 contains the original set of drawings used to manufacture the ATC.

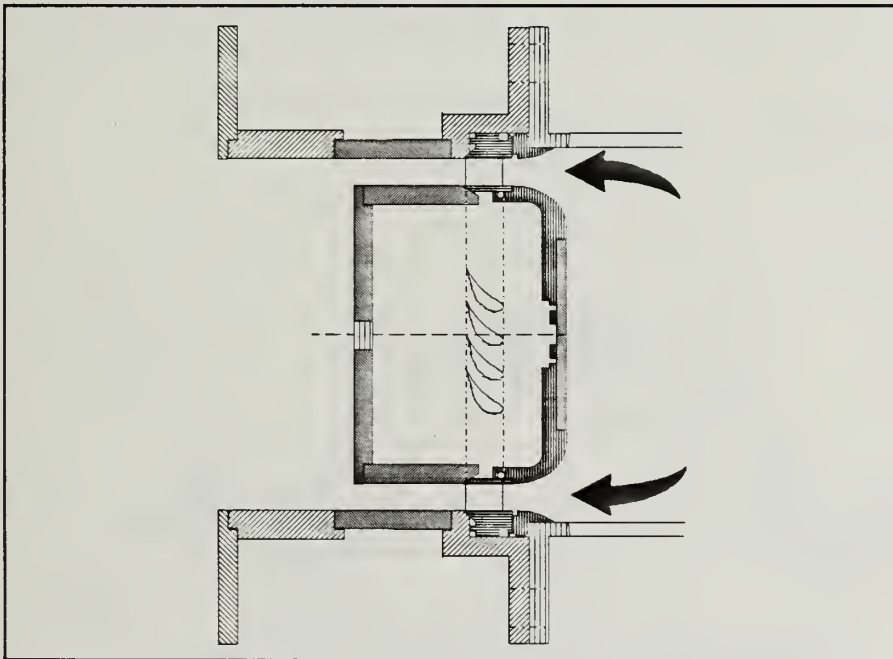


Figure 2. Annular Turbine Cascade Cutaway

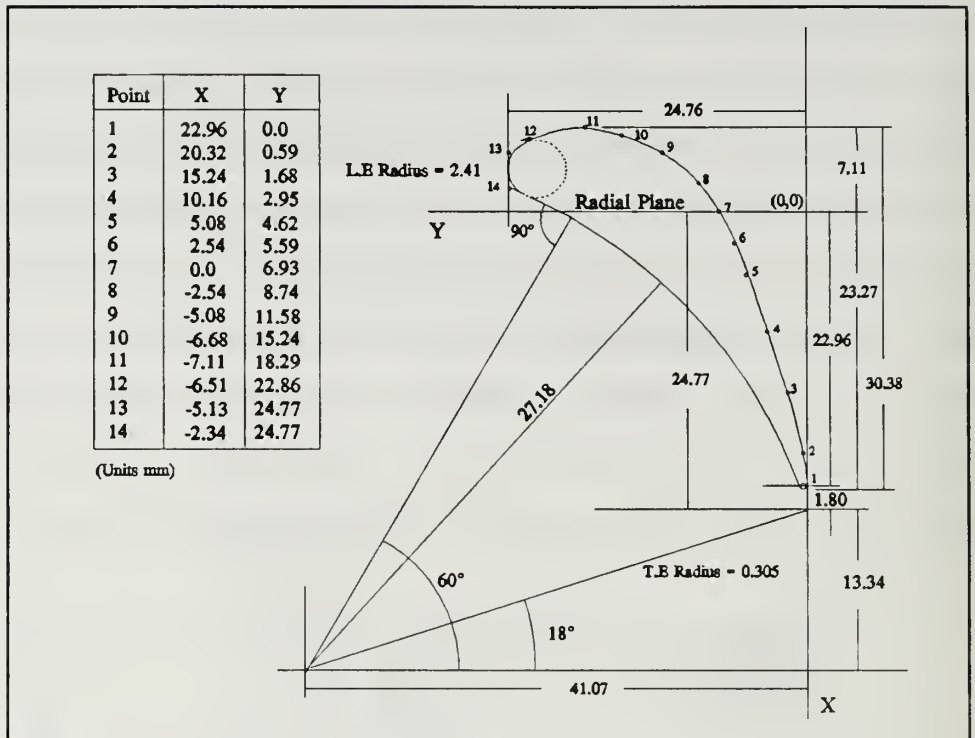


Figure 3. Blade Geometry

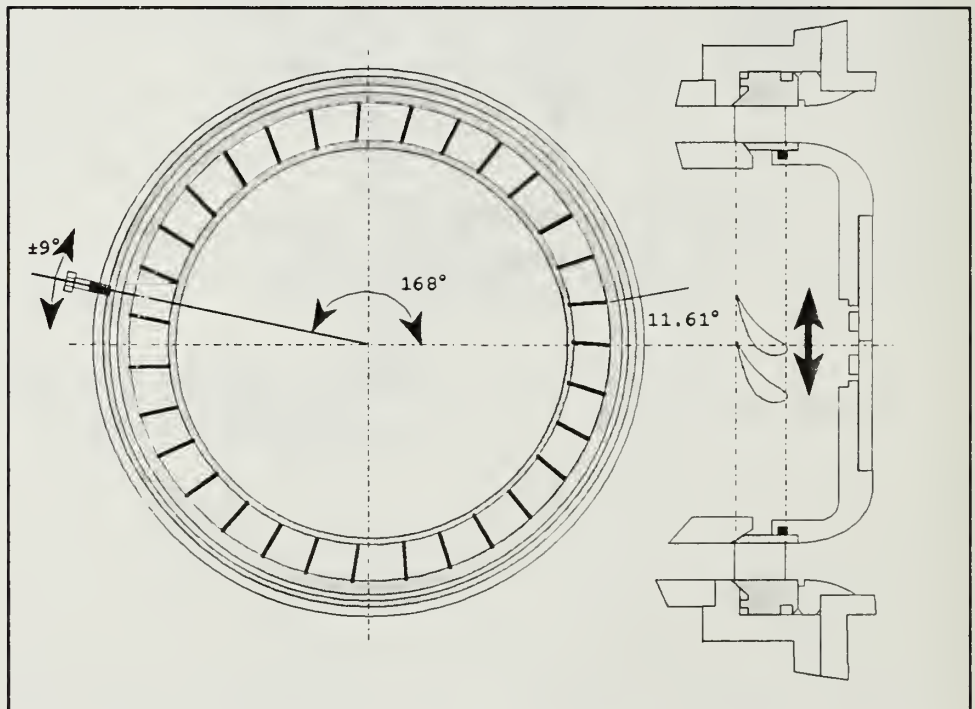


Figure 4. Wake Positioning System

2. PRESSURE MEASUREMENT MODIFICATIONS

The original ATC pressure measurement access was located two axial chords downstream of the blade trailing edges. Figure 5 details the old and new probe holes. The outer casing was modified to accommodate the half-chord access hole and is shown in conjunction with the adjustable holder. A new set of static pressure ports was added to the inner hub as shown. The ports were set 90 degrees apart and in axial alignment with the original holes. Tubing was connected to provide an average pressure tap for both hub axial locations. Appendix A contains a complete set of the drawings used for machining.

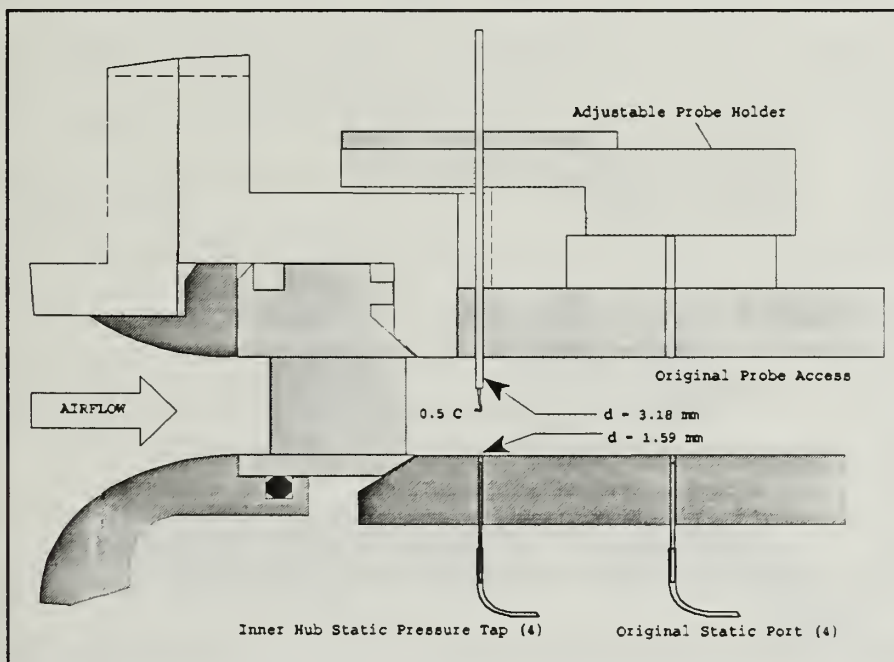


Figure 5. Pressure Measurement Changes

3. LDV MODIFICATIONS

LDV access was changed to minimize light reflection and improve off-axis options. The desire to ultimately obtain a third component necessitated an offset angle for a second fiber-optic probe. The design allowed for simple removal and replacement of the window during operation for cleaning, and radial access as shown in Figure 6. The position of the wake relative to the probe volume was controlled externally by rotating the blade row, inlet bellmouth and center body ahead of the measurement volume. An alignment blank was used to orient the laser traverse axis to the ATC. The 1.0922 mm (0.043 in) diameter hole in the blank provided an endwall flow measurement capability as shown in Figure 7.

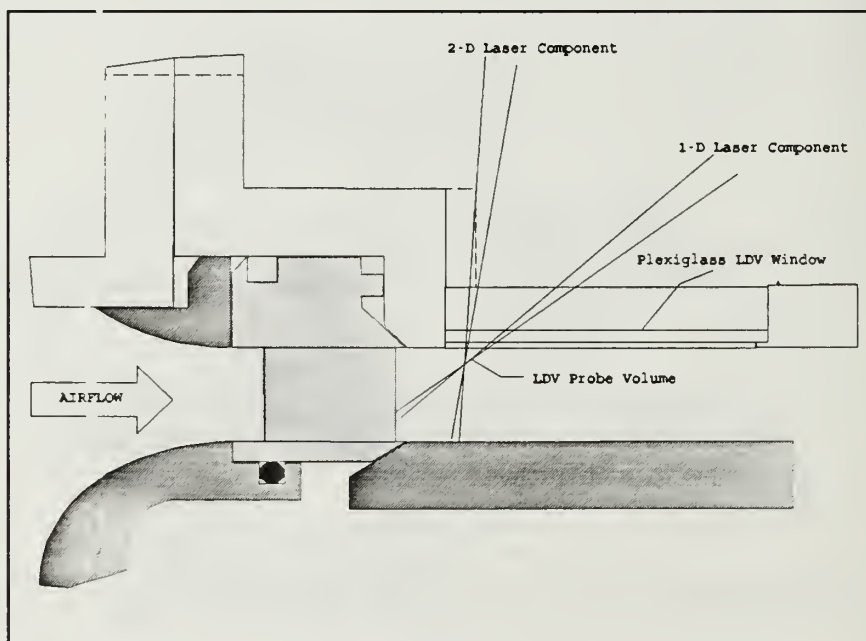


Figure 6. LDV Access Modifications

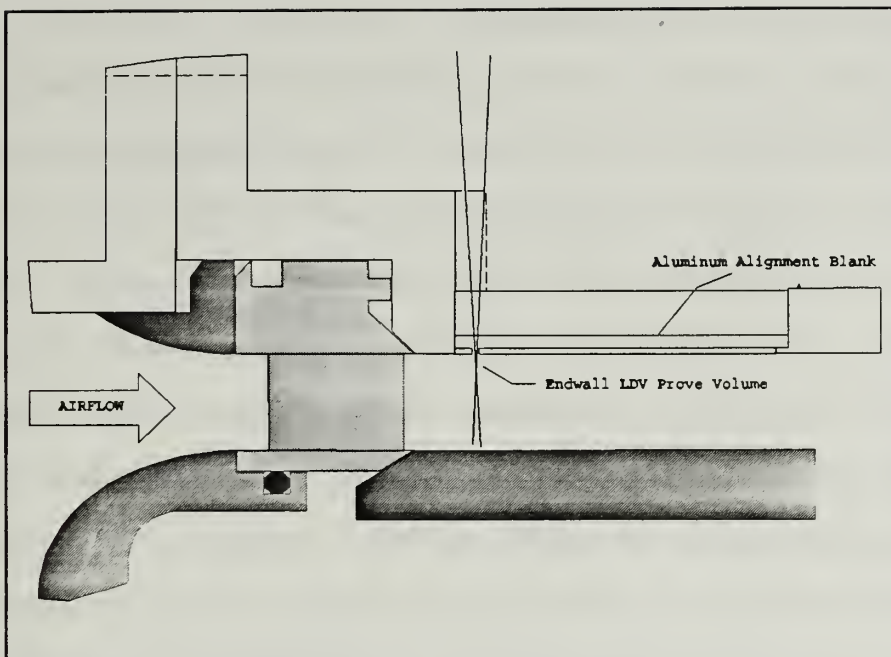


Figure 7. Endwall Measurement Technique

C. PRESSURE PROBE

Total pressure, Mach number and flow angle measurements were made with a three hole yaw probe [Ref 4]. All pressure taps were connected to a Scanivalve with a ± 344 kPa (± 50 psi) differential transducer. Scanivalve control and data recording were accomplished using an HP-9000 computer system. Appendix B contains calibration curves and a listing of the Hewlett-Packard code used to acquire and output data. Pressure data from the ATC were acquired with the same hardware and software used in the probe calibration.

Previously, yaw alignment was accomplished using a "U"-tube water manometer. Difficulty encountered with hysteresis and the response of the water to yaw misalignment was corrected with the use of a differential pressure transducer.

D. LASER-DOPPLER VELOCIMETER

The LDV system is shown schematically in Figure 8. The Lexel Model 95 four-Watt Argon-Ion LASER was connected to a TSI, Inc., Model 9201 ColorBurst Multicolor Beam Separator. The beam separator split the incoming light into two beams, with one beam passing through a Bragg cell for 40 Mhz frequency shifting. The two beams were further split into three polarized pairs: green (514.5 nm), blue (488 nm), and violet (476.5). The TSI, Inc., Model 9230 ColorLink Multicolor Receiver provided the frequency-shift signal to the ColorBurst for beam shifting. Each beam was directed through individual couplers for transmission to the laser probe by fiber-optic cable. The fiber-optic probes contained receiving optics to direct the return signals to the ColorLink.

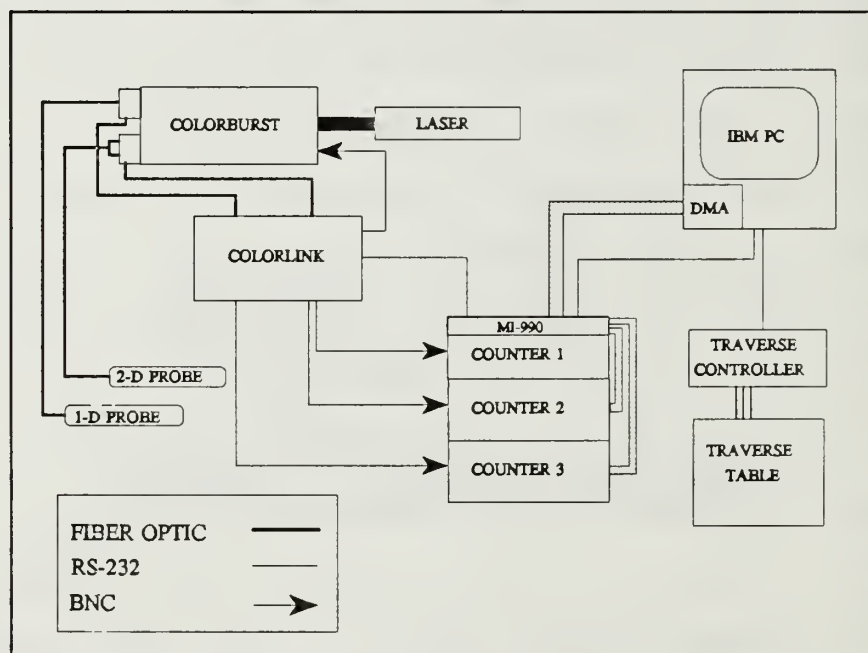


Figure 8. LDV Wiring Schematic

The ColorLink provided photomultiplier and frequency shifting functions. Control of shifting and photomultiplier voltage was accomplished remotely by computer. After conditioned by the ColorLink, the signals were sent to individual TSI, Inc., Model 1990C signal processors where valid Doppler signals were counted with reference to desired characteristics set by the user. An MI-990 interface monitored coincidence criteria (2-D measurements) and transferred valid counter information to computer memory.

The fiber-optic probes were mounted to a Model 41583 LINTECH Traverse Table. An Applied Motion Products System 1618 Traverse Controller was used to control traverse movement manually and by computer. [Ref. 5] All remote control of LDV system equipment and data processing was completed through the menu driven environment of TSI's FIND version 4.04.

E. EXPERIMENTAL PROCEDURE

1. PROBE CALIBRATION

Probe calibration and investigation of data acquisition options were completed together. The calibration was accomplished using a free-jet with a 107.9 mm (4.25 in) nozzle connected to the air supply (Figure 1) used for the annular cascade. Figure 9 shows the testing apparatus and pressures used to calibrate the cobra probe.

The probe was aligned in yaw with a ± 68.9 kPa (± 10 psi) Stathan, SCO 277-10, differential pressure transducer.

Yaw-alignment response was an improvement over the previous manometer arrangement. The transducer bridge output was periodically zeroed by removing the probe from the flow. The yaw pressure measurement was tapped from one side of the transducer as shown in Figure 9. The Scanivalve system recorded the five pressures shown in Figure 9. Pre-operation tubing-leak checks were completed by trapping pressure to each Scanivalve port in turn.

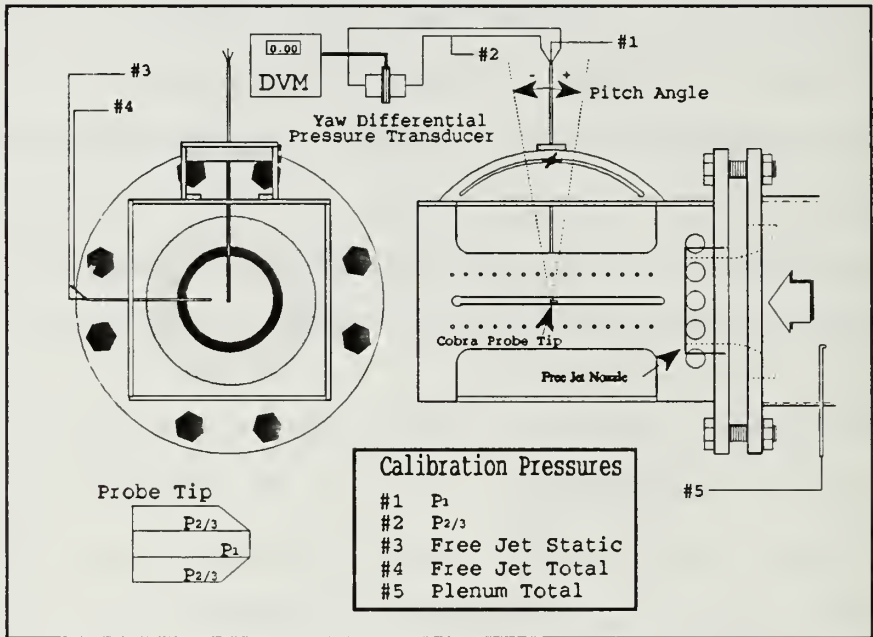


Figure 9. Yaw Probe Calibration Equipment

The probe was calibrated at Mach numbers from 0.20 to 0.79 in steps of 0.1. Pitch sensitivity was investigated at twelve positions from minus ten degrees to plus eight degrees (Figure 9). Appendix B contains a description of the calibration variables and shows the sensitivity of the probe

to pitch angle. Sixth-order polynomials were fit to the calibration data. The zero-degree probe calibration was successfully validated (Appendix B) under different atmospheric conditions.

2. PRESSURE PROBE MEASUREMENTS

Wakes were surveyed by repositioning the blade passage upstream relative to the probe. The inner hub rotated with the blade ring as the wake was positioned for LDV or pressure measurement. The bolt shown in Figure 4 was used to position and hold the inner ring and stator. A total of 18 degrees circumferential variation, in steps of one degree, was achieved.

Cobra-probe measurements were completed as described in the calibration section. Upstream static and stagnation, and inner-hub static pressures were used in conjunction with the center-port and yaw-port pressures of the probe. The probe provided total pressure and flow angle. Mach number was obtained from β (Appendix B). The desired hub-static to upstream-stagnation pressure ratio was set using the Scanivalve system and manual control of the air supply dump valves. The probe was positioned radially and aligned with the flow before pressure data were acquired. Upstream stagnation temperature and wake flow angle were recorded manually for each measurement location. Flow angle was read from a vernier scale to an accuracy of plus or minus 0.2

degrees at span locations greater than 25 percent. Span position was established with reference to 100 percent at the outer wall.

3. LDV ALIGNMENT

LDV alignment for endwall flow measurement was attempted as shown in Figure 10. The laser mounting bracket micrometer was set to ten millimeters for visual alignment around the access hole as shown. Obtaining a repeatable depth reference was not possible. This alignment technique did provide micrometer scale coverage for data recording and ensured the beams passed cleanly through the hole. The length of the probe volume precluded the use of the outer surface of the plate as a reference point.

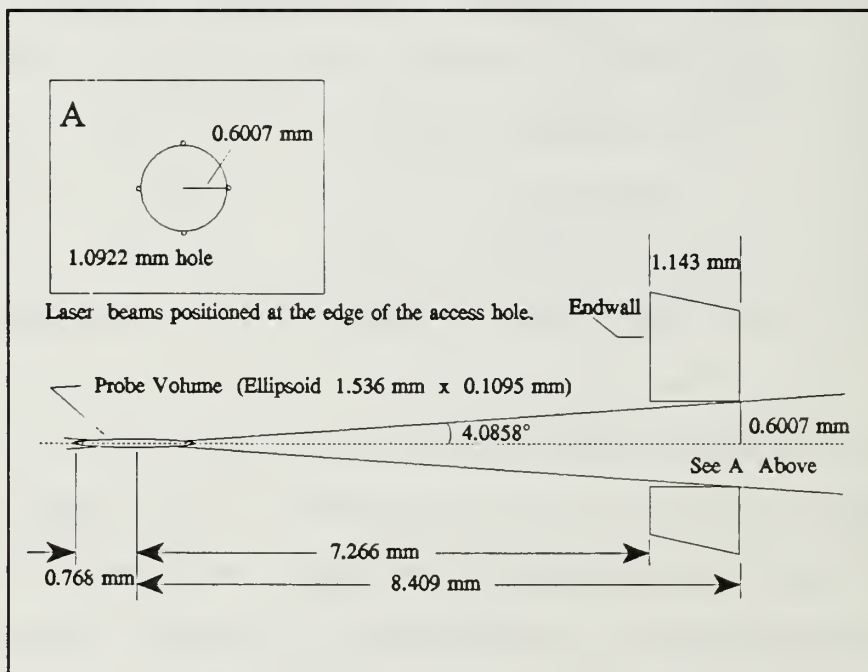


Figure 10. Endwall LDV Alignment Technique

Alignment for automatic traverse of the wake passage through the window was accomplished using the alignment blank (Figure A8). The multi-component beams were positioned in each of the six alignment holes using manual control of the traverse table. The coordinates were read from the digital position indicator on the traverse controller for each hole. Axis conversion from the traverse to the ATC was completed using the position data and the dimensions of the alignment blank (Appendix A). Traverse table movement could then be programmed using the automatic traverse control menu in TSI's FIND software.

4. ENDWALL MEASUREMENTS

Endwall flow data were acquired without the use of automatic traverse control. The laser beams were aligned with the half-axial-chord access hole as described above, and then traversed manually using the probe-bracket micrometer. Adjustments to seeding position, counter gain and photomultiplier voltages were continually updated to maximize data rate and minimize the effect of noise. Seed-wand position was particularly important. Micrometer position information was married to the appropriate data files in post processing of FIND's output ASCII .PRN files using Borland Corporation's spreadsheet program Quattro Pro version 5.0.

III. COMPUTATIONAL FLUID DYNAMICS

A. GRID GENERATION

Grid generation was completed using Turbomachinery C GRID, TCGRID, [Ref. 6]. The code was developed to build 3-D "C" or "H" type grids for turbomachinery in the standard PLOT3D format (NASA Ames Research Center graphics software). Appendix C contains the namelist input file used to generate the stator geometry and a discussion of the output. The inlet bellmouth and center body as shown in Figure 4 were not modeled for this study.

Careful manipulation of the namelist variables was required to obtain a smooth solution. The grid geometry was developed to improve resolution of the endwall boundary layer. The ability to generate a fine grid was hampered severely by the length of wake desired in the model. Reduction of the wake-exit plane from one axial chord downstream of the blade trailing edges [Ref. 4] to one-half axial chord resulted in a dramatic increase in grid resolution. The final grid dimension was 150x31x65, up from 121x31x21. The blade surface received an additional 29 points and the radial resolution was improved from 21 points to 65. The smaller computational wake length also reduced the interval between grid lines from the trailing edge of the blade.

B. COMPUTATIONAL SCHEME

Flow solutions were completed using Rotor Viscous Code 3-D (RVC3D). RVC3D [Ref. 7] was designed to solve three-dimensional viscous flows in turbomachinery. The code solves thin-layer Navier-Stokes equations in Cartesian coordinates using an explicit finite difference technique. Turbulence effects were modeled using the Cebeci-Smith option. The restart option of the code was utilized throughout the investigation to monitor convergence of the solution. Appendix D contains the namelist input file used to obtain the final solution and a description of steps required to run the code on the Naval Postgraduate School (NPS) Cray computer. Output solution files (fort.3) were examined using the graphics software PLOT3D. Comparison with experiment required data reduction of the output file. Appendix E contains a synopsis of the output file structure with data reduction steps required for comparisons and a listing of the FORTRAN program (plane.f) used to accomplish the manipulation.

The final solution selected for comparison was chosen for the minimum residual and the smoother transition of a solution across the wake cut. An area of unsteady flow became prominent near the hub and on further analysis revealed an area of predicted reverse flow. Figure 11 contains a comparison between total pressure ratio results at the 50 percent span location for 1200 and 1490 iteration solutions.

One blade wake is shown with the wake cut in the grid clearly evident in the plot. The closely-spaced points in the wake cut of the TCGRID geometry has introduced a mathematical boundary. The 1200 iteration solution exhibited the beginning of the reverse flow area near the hub, but contained serious discontinuities because of the solution scheme. The 1490 iteration total-pressure-ratio plot demonstrates the smoothing that took place as the solution progressed.

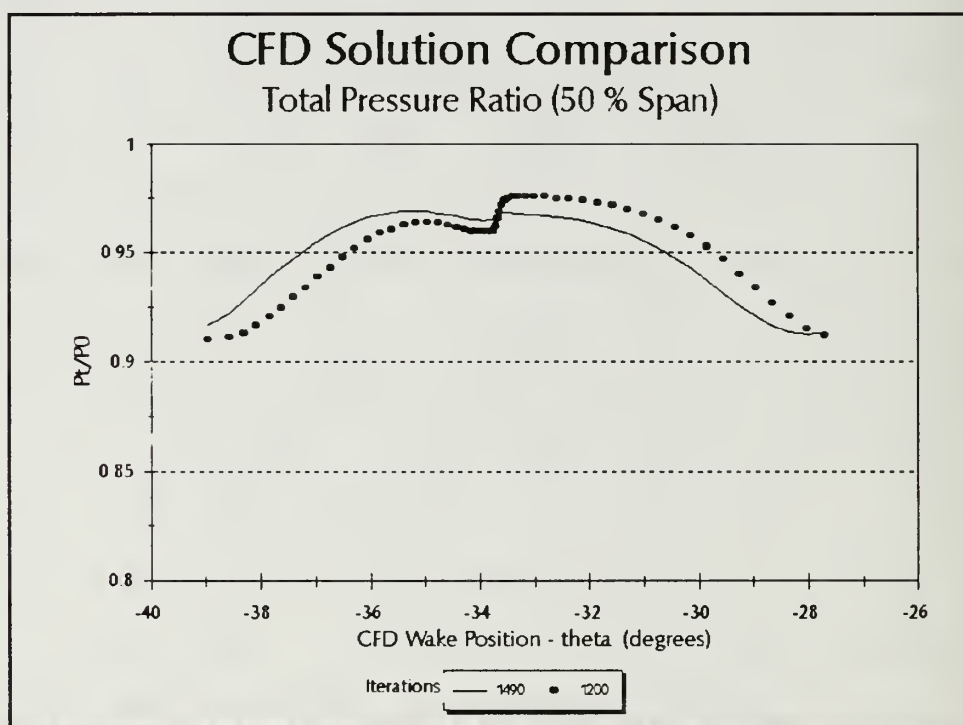


Figure 11. CFD Solution Comparison, 50% Span

IV. RESULTS AND DISCUSSION

A. PRESSURE PROBE

Annular Turbine Cascade pressure measurements were obtained at an average Reynolds number of 650000 based on axial chord. The pressure ratio, inlet total to exit static at the hub, was set at 0.68 to enable a proper comparison to be made with the CFD solution. Pressure and flow angle measurements were repeatable, with Scanivalve pressure-acquisition standard deviations of less than 0.20 percent. However, data obtained inside 25 percent span were at low dynamic pressure and too difficult to resolve with the pressure probe, and are therefore not reported. Flow unsteadiness increased as the probe was immersed further in from the endwall. The direction of approach to zero yaw in the less-than-25-percent span region affected the flow angle measurement by as much as 0.5 degrees.

Pressure and flow-angle data were taken at 18 wake positions for 25, 50, 75 and 90 percent span locations on the half-axial-chord wake measurement plane. Pressure data repeatability was demonstrated along the 50 percent span station for all wake positions, and radially at the two-chord zero-degree wake position. Figure 12 shows the total-pressure-ratio data obtained for the 50 percent span location.

The data show that there was a negligible influence of the conical diffuser. Figure 13 shows the repeatability obtained in radial surveys for a constant wake position at the two-chord measurement location. The repeatability shown in Figures 12 and 13 clearly validated the ability to reset the desired operating pressure ratio for the experiment. Flow angle measurements were repeated at the 90 percent span location, and radially at the two-chord wake measurement location as shown in Figures 14 and 15. In all cases, the repeatability of the probe pressure measurements was excellent, with the largest discrepancy less than 0.5 percent in total pressure.

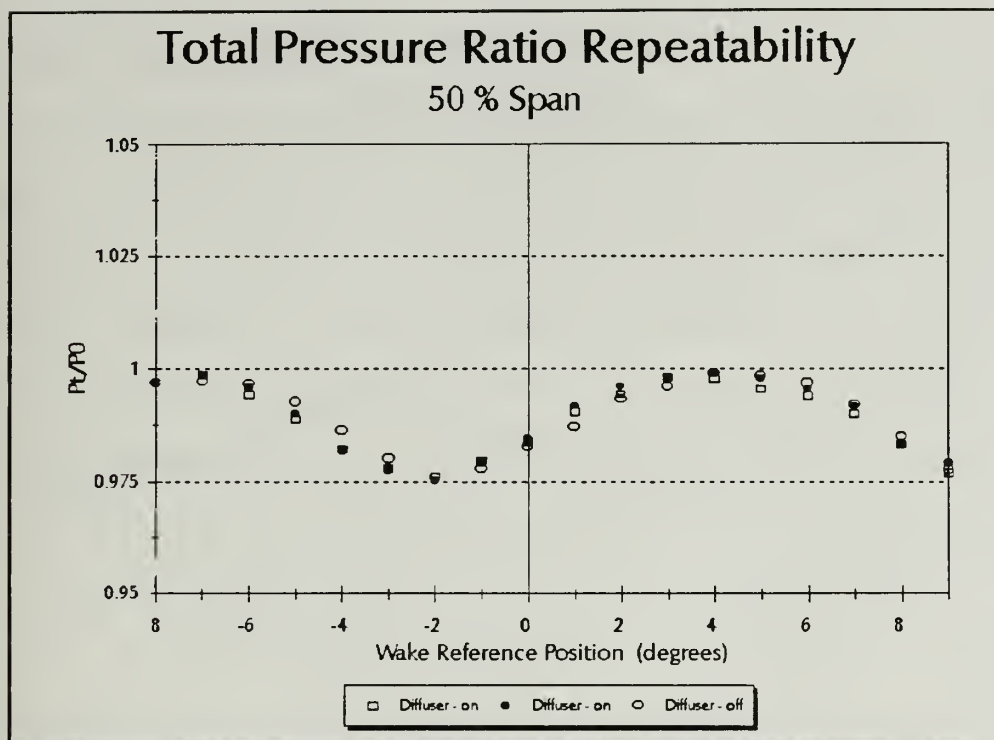


Figure 12. P_t/P_0 Repeatability, 50% Span

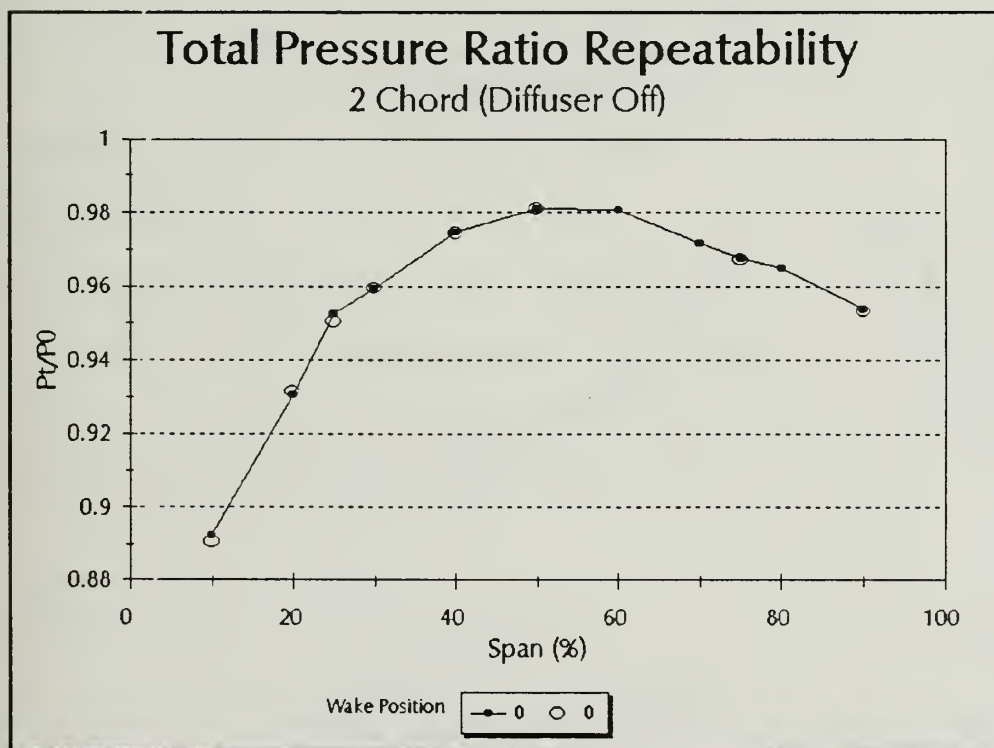


Figure 13. P_t/P_0 Repeatability, Radial

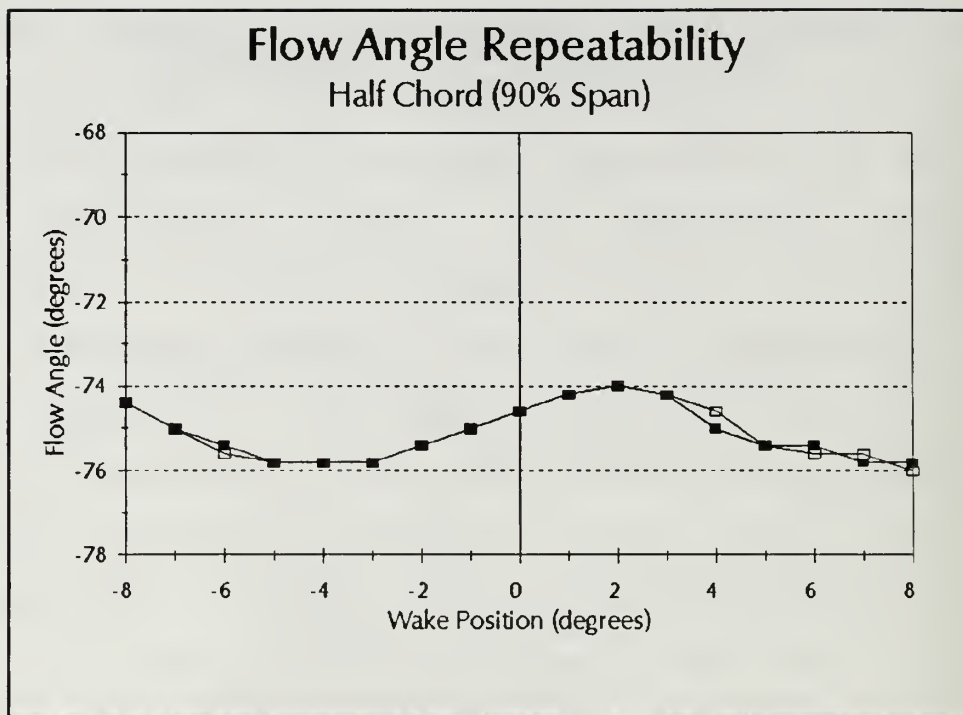


Figure 14. Angle Repeatability, 90% Span

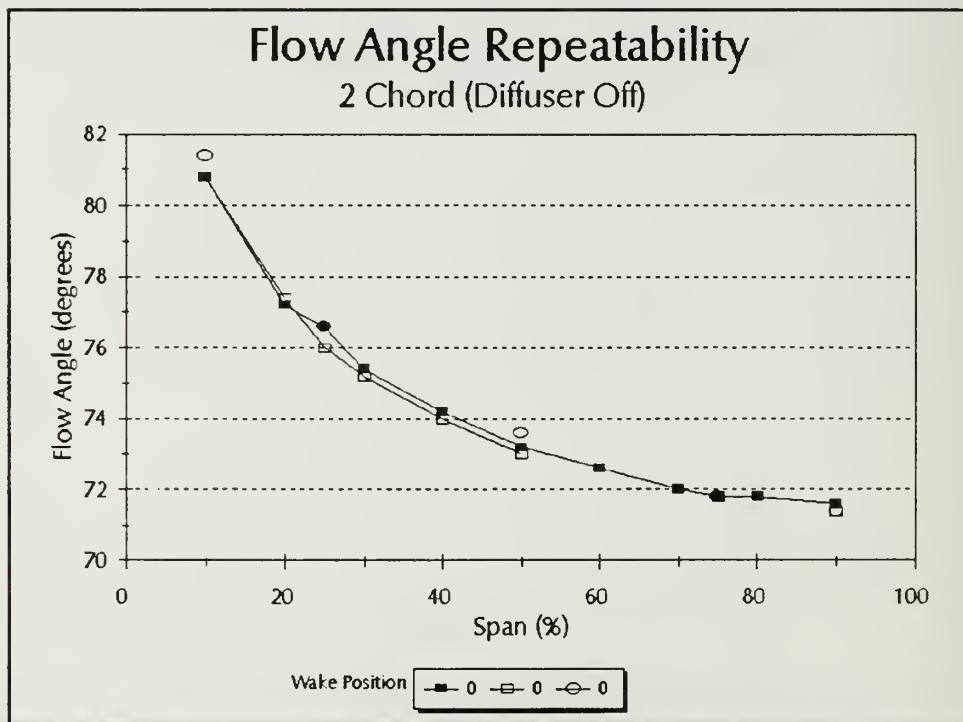


Figure 15. Angle Repeatability, Radial

B. LASER MEASUREMENTS

Two-dimensional LDV measurements were obtained through a 1.0922 mm (0.043 in) hole to a depth of approximately three millimeters. Initial measurements were taken with one component (green) of the two-component probe. Figures 16 and 17 show the velocity profile and turbulence intensity results from the first attempt at endwall measurements. The 'depth' shown in the graphs is an estimated distance from the endwall based on the rapid loss of data rate observed at the depth shown as 0.1 mm from the endwall. The data map a boundary layer profile to approximately 0.6 millimeters. The high pressure ratio (0.98) provided near perfect seed conditions, and the casing vibrations were low. The data shown for V-z do not necessarily coincide with the exact locations of the data for V- θ because the fiber-optic probe was rotated 90 degrees and alignment could not be maintained.

The turbulence intensity results are with respect to the maximum velocity at the furthest measurement location into the annulus. The significantly higher turbulence intensity in the V- θ direction is probably due to the steep gradient of the V- θ mean-flow profile in the radial direction.

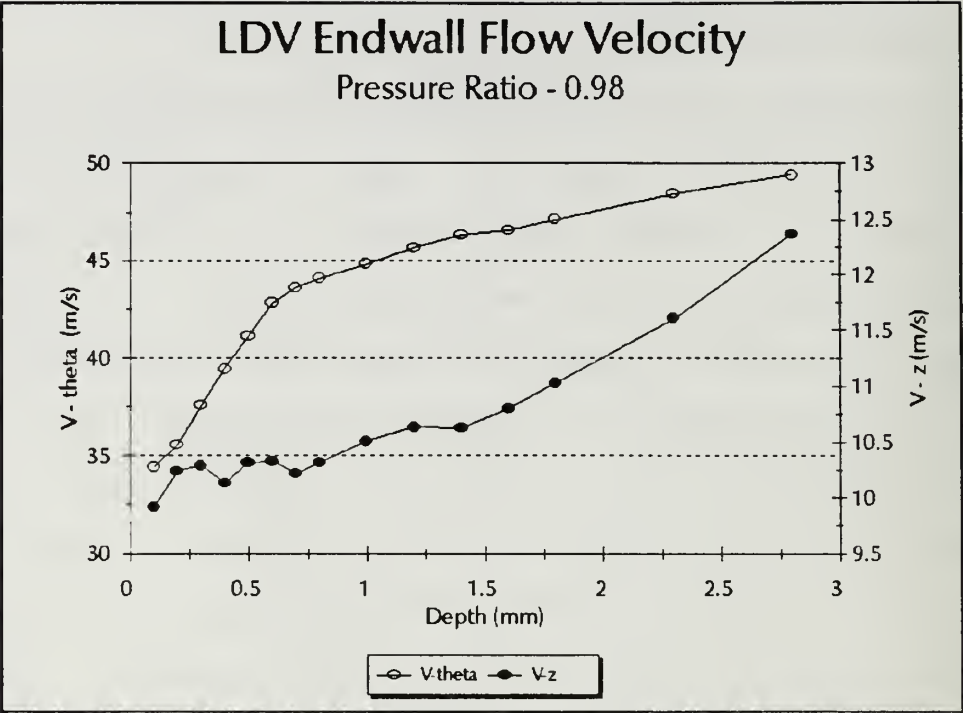


Figure 16. Single Component LDV Endwall Velocity

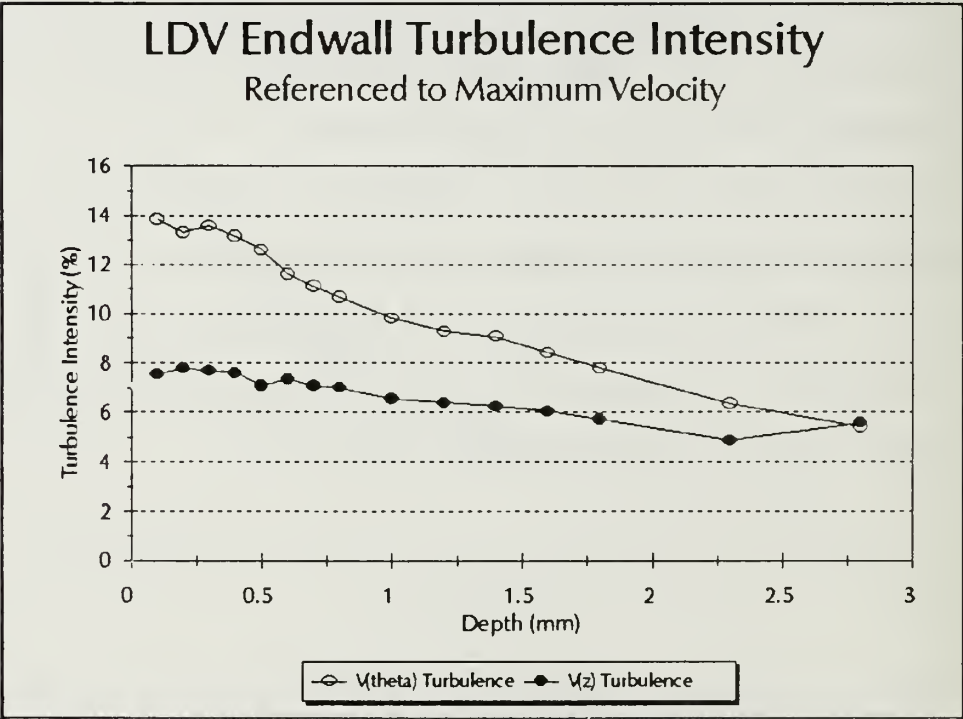


Figure 17. Single Component LDV Turbulence

Two component LDV measurements were obtained at approximately 15 percent higher flow velocity. Figure 18 depicts a test section 'sweep' of near-endwall velocity measurements at a pressure ratio of 0.974. Depth reference (in mms with respect to an unknown datum on a vernier scale) is shown. The exact distance from the wall was not obtainable. Flow periodicity is suggested and decreasing velocities toward the outer casing show the endwall boundary layer. The boundary layer is distorted due to corner vortices and secondary flows that originate in the blade row. Flow angle and turbulence intensity plots are included in Figures 19 through 21. Once again the turbulence intensity in the V- θ direction is higher than that in the V-z direction. Figures 18 through 21 represent automatic editing of the histograms by the FIND software (user selection). Data outside two standard deviations were discarded.

Increased flow velocity introduced higher vibration levels and temperature increases as the test progressed. Hole alignment was periodically verified and, occasionally, small adjustments (less than 0.01 mm) were required.

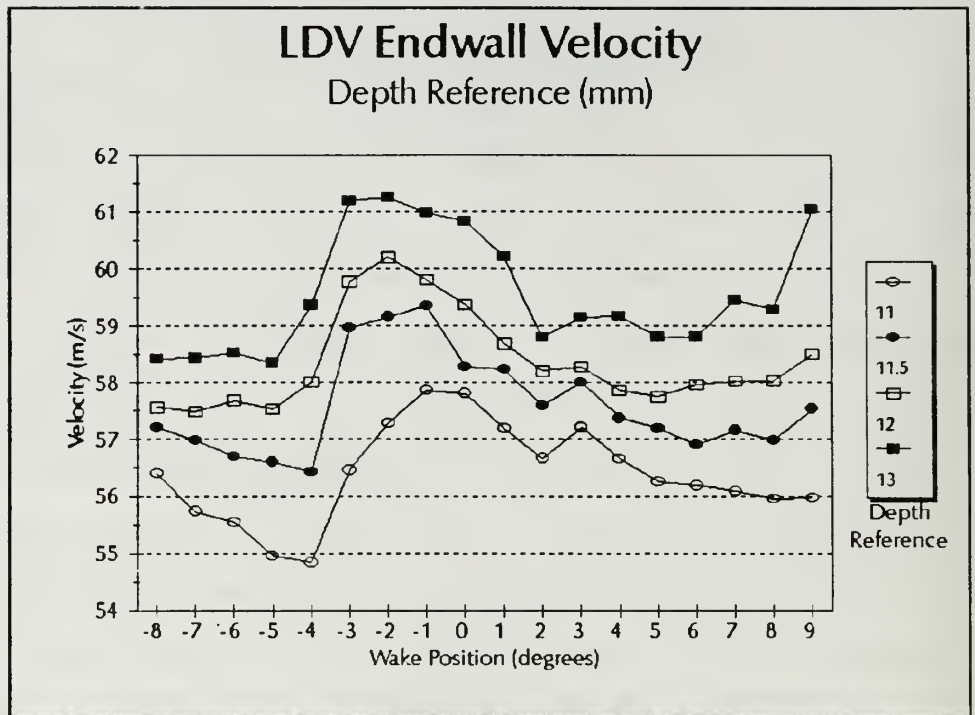


Figure 18. Two Component LDV Endwall Velocity

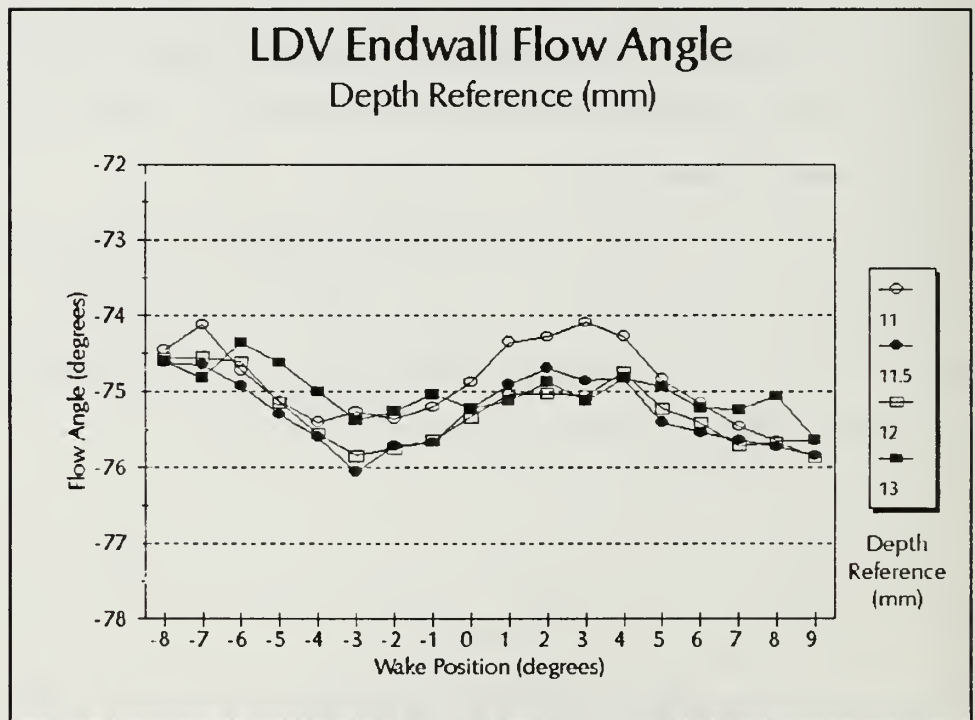


Figure 19. Two Component LDV Flow Angle

Vtheta Turbulence Intensity Referenced to Maximum Velocity

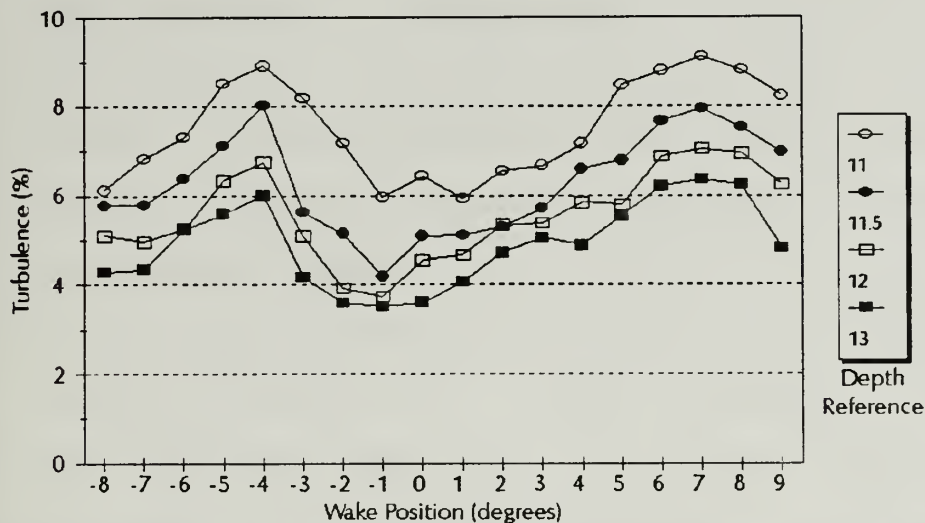


Figure 20. Two Component LDV Turbulence, V-theta

Vz Turbulence Intensity Referenced to Maximum Velocity

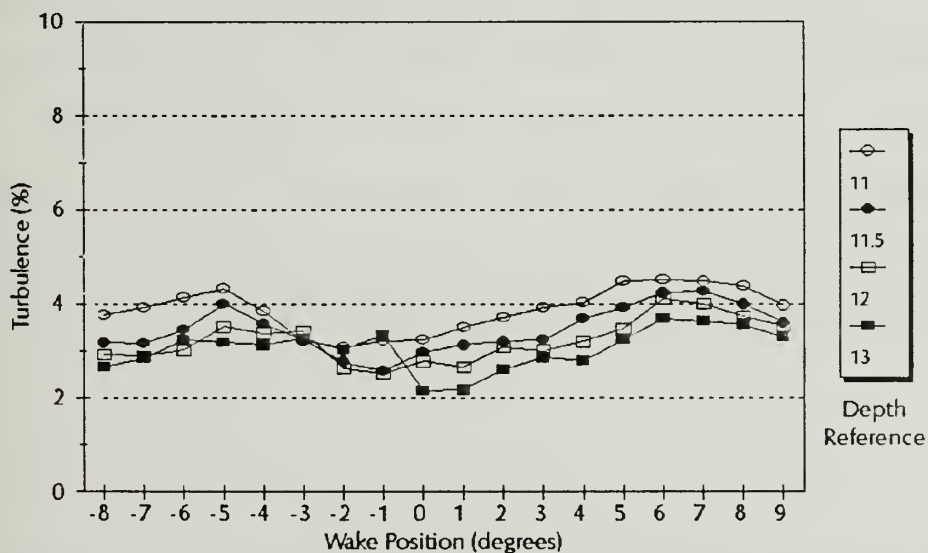


Figure 21. Two Component LDV Turbulence, V-z

C. NUMERICAL RESULTS

The CFD solution was run with the same pressure ratio (0.68) used in the experiment. Graphical output of the numerical results was useful in obtaining a qualitative understanding of the flow characteristics. Figure 22 depicts the predicted pressure ratio for the blade surface at the hub, mid-span and tip. The suction surface curves suggest that the position of the blade passage throat was at 0.8 of axial chord. Figure 23 shows, with colored contours, pressure coefficient information for the blade surface pressure distribution. The Mach number contours shown in Figure 24 provided an initial indication of where flow characteristics were well established. Boundary layers appear as expected, thin near the endwall and thick near the hub. Wake curvature in the spanwise direction is also evident in the Mach contour plot. Difficulty in obtaining repeatable flow angles in the experiment below 25 percent span may have been due to the unsteady flow separation which is suggested by the computational results for the region near the hub wall. However, the reverse flow predicted by the code in this region could not be verified in the experiment.

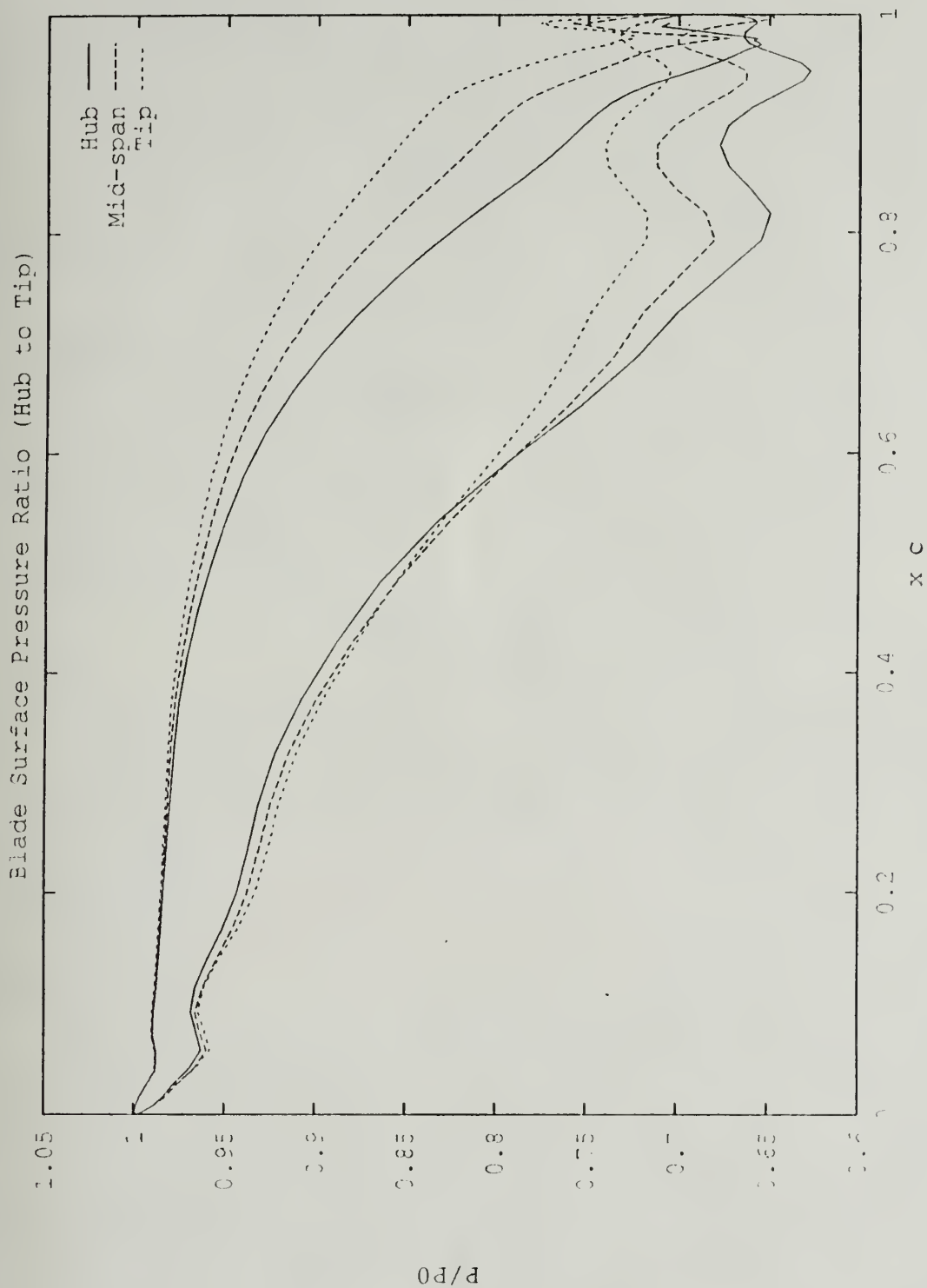


Figure 22. RVC3D Blade Pressure Ratio Plot

PRESSURE COEFFICIENT

MACH
ALPHA
Re
TIME
GRID

0.130
0.00 DEG
6.65x10**6
1.49x10**3
150 x31 x65

CONTOUR LEVELS

-33.0000
-32.0000
-31.0000
-30.0000
-29.0000
-28.0000
-27.0000
-26.0000
-25.0000
-24.0000
-23.0000
-22.0000
-21.0000
-20.0000
-19.0000
-18.0000
-17.0000
-16.0000
-15.0000
-14.0000
-13.0000
-12.0000
-11.0000
-10.0000
-9.00000
-8.00000
-7.00000
-6.00000
-5.00000
-4.00000
-3.00000
-2.00000
-1.00000
0.00000
1.00000



Figure 23. PLOT3D Blade Pressure Coefficient Plot

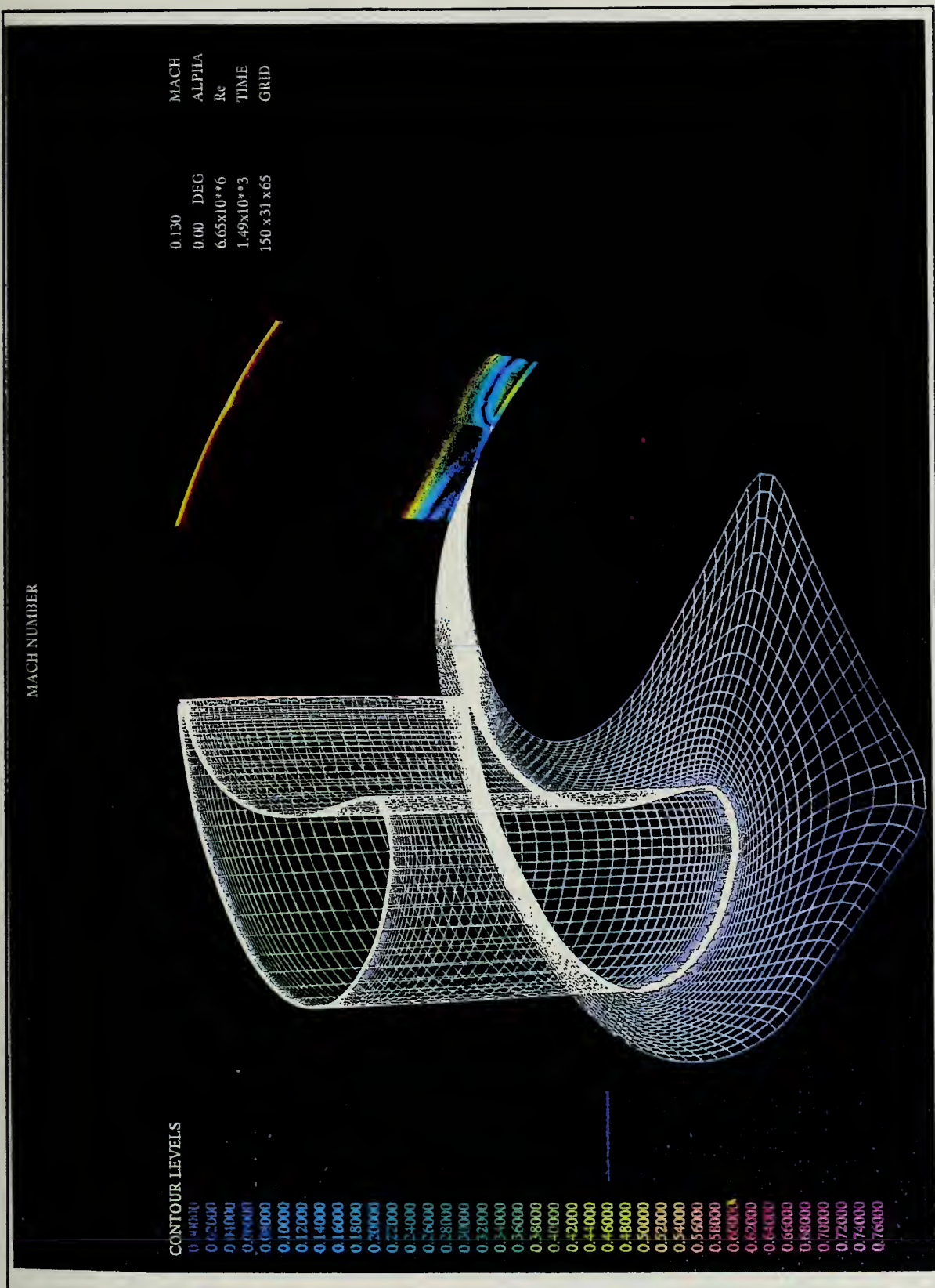


Figure 24. PLOT3D Exit Plane Mach Contour Plot

D. COMPARISON

Three comparisons were made between numerical and experimental results. To show the flow periodicity, the CFD solutions were repeated over two blade passages as shown by the solid line in the following Figures 25 through 36. Comparisons between experiment and numerical (Appendix E) results are presented for total pressure ratio, Mach number and flow angle. Figures 25 through 28 show the total pressure ratio comparison. It is noted that uncertainty in the probe measurement of total pressure is small. The probe calibration uncertainty enters only when comparing Mach number. Wake-profile phase coincidence was established using the 50 percent span Mach number data. The phase was kept constant for the circumferential comparisons at all other spanwise locations. Mach number (Appendix B) comparisons are contained in Figures 29 through 32, and Figures 33 through 36 contain the flow angle data.

CFD total pressure ratio predictions were within 10 percent of the experimental values at 25 percent span. The difference decreased to below one percent at 90 percent span. Mach number comparisons with measurements were within 15 percent at 25 percent span and decreased to three percent at 90 percent span. Flow angle comparisons were within five degrees at 90 percent span with improvement to within two degrees at 25 percent span. The reason for closer agreement

in total pressure ratio and Mach number toward the tip and improving agreement in flow angle toward the hub is unexplained.

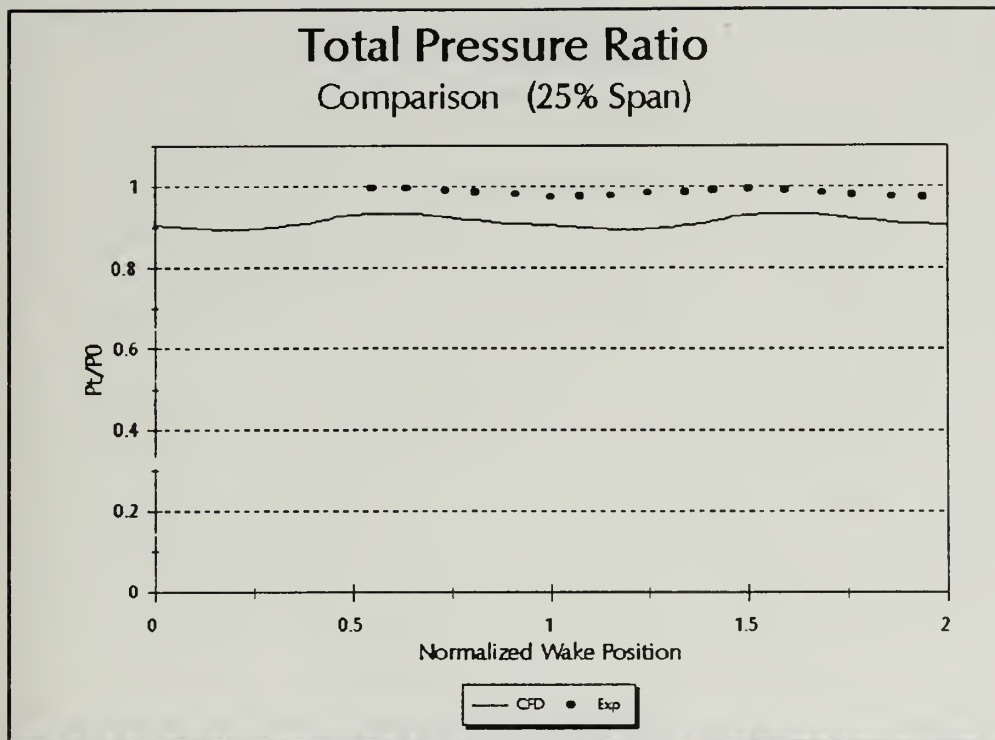


Figure 25. Total Pressure Ratio Comparison, 25%

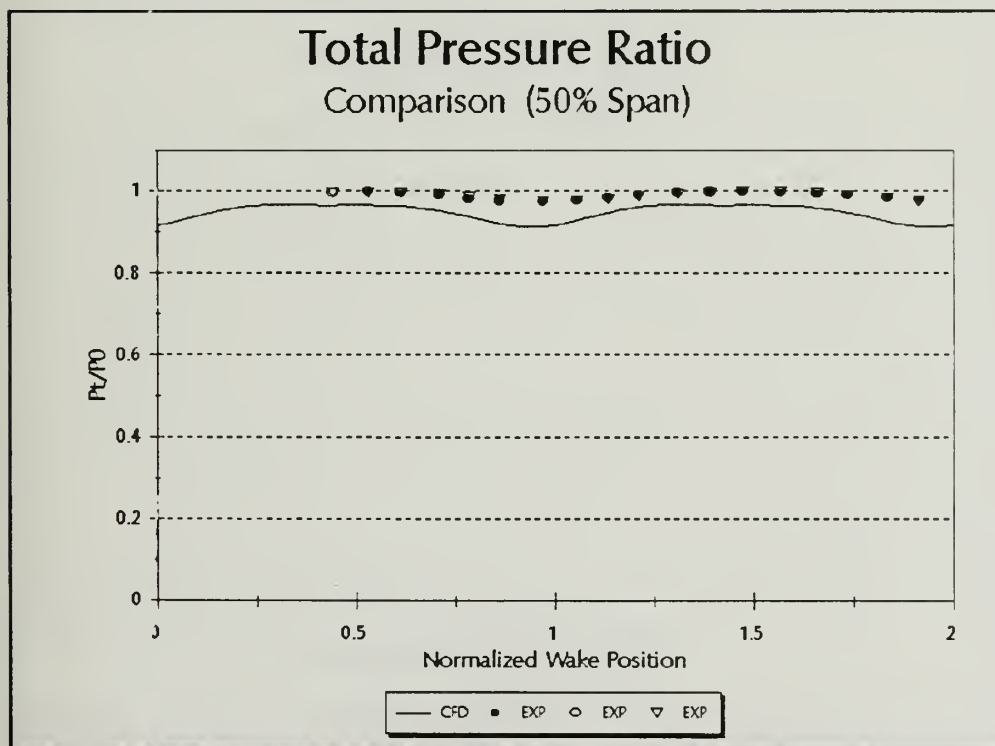


Figure 26. Total Pressure Ratio Comparison, 50%

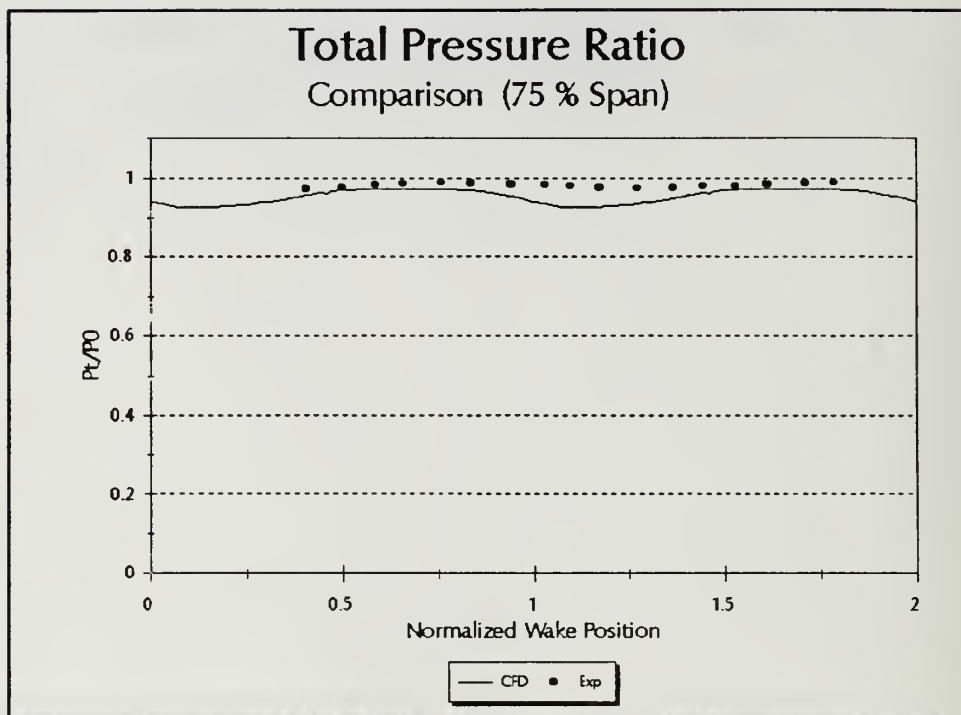


Figure 27. Total Pressure Ratio Comparison, 75%

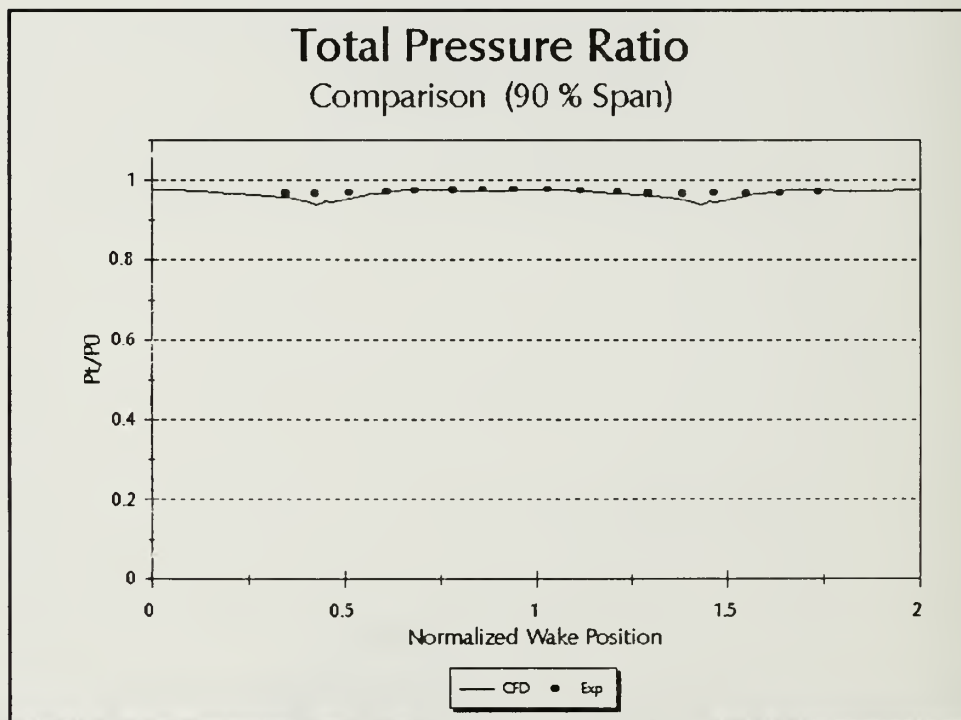


Figure 28. Total Pressure Ratio Comparison, 90%

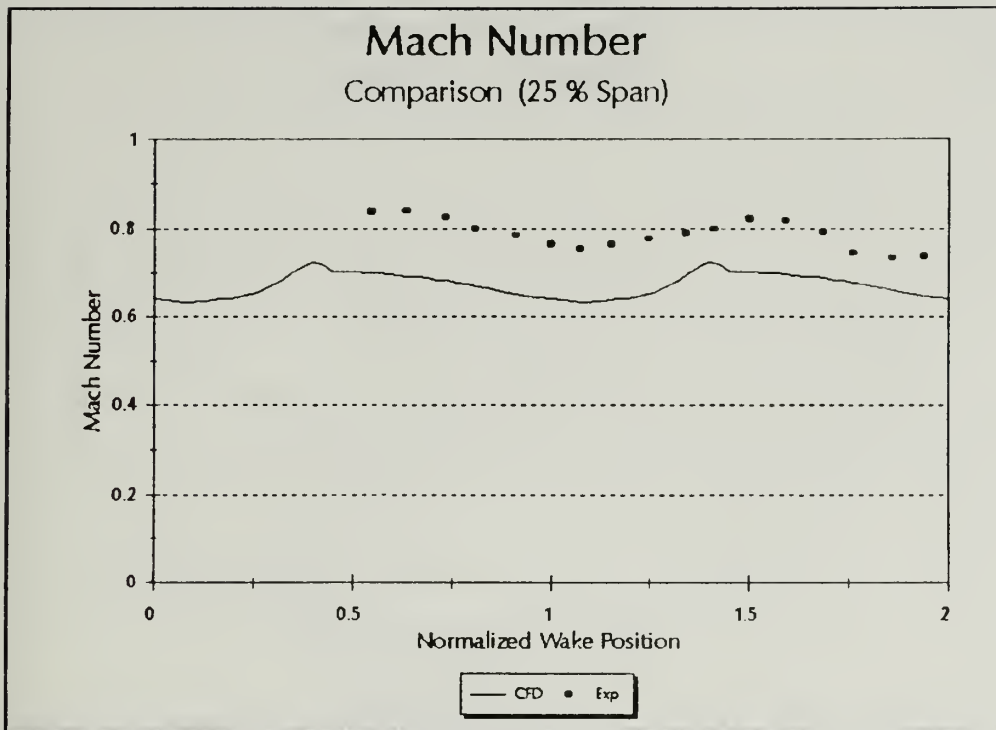


Figure 29. Mach Number Comparison, 25%

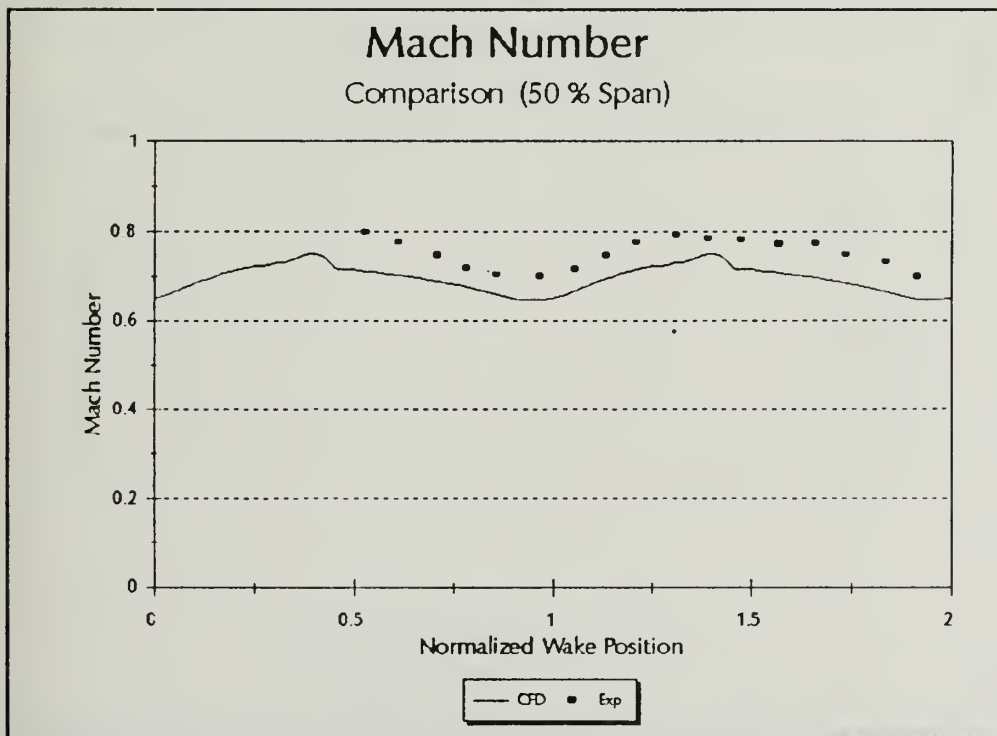


Figure 30. Mach Number Comparison, 50%

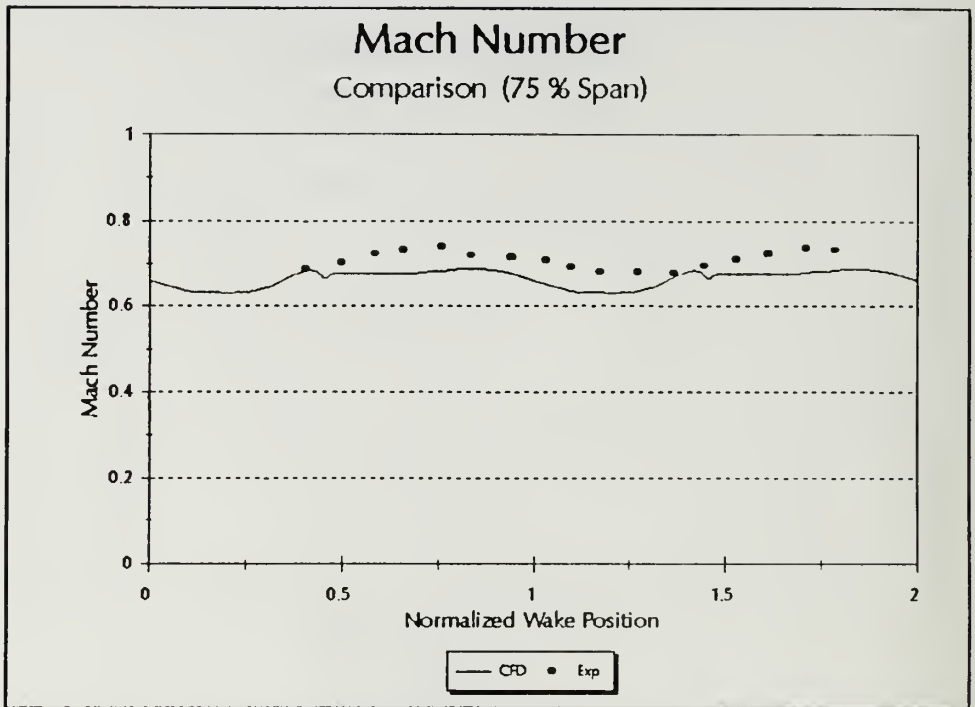


Figure 31. Mach Number Comparison, 75%

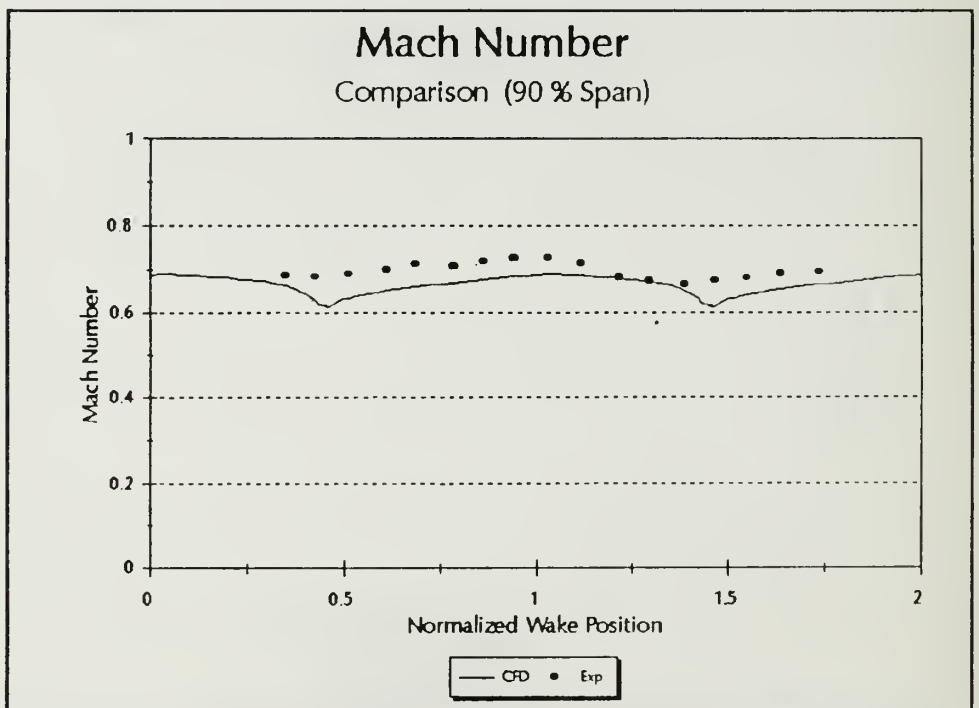


Figure 32. Mach Number Comparison, 90%

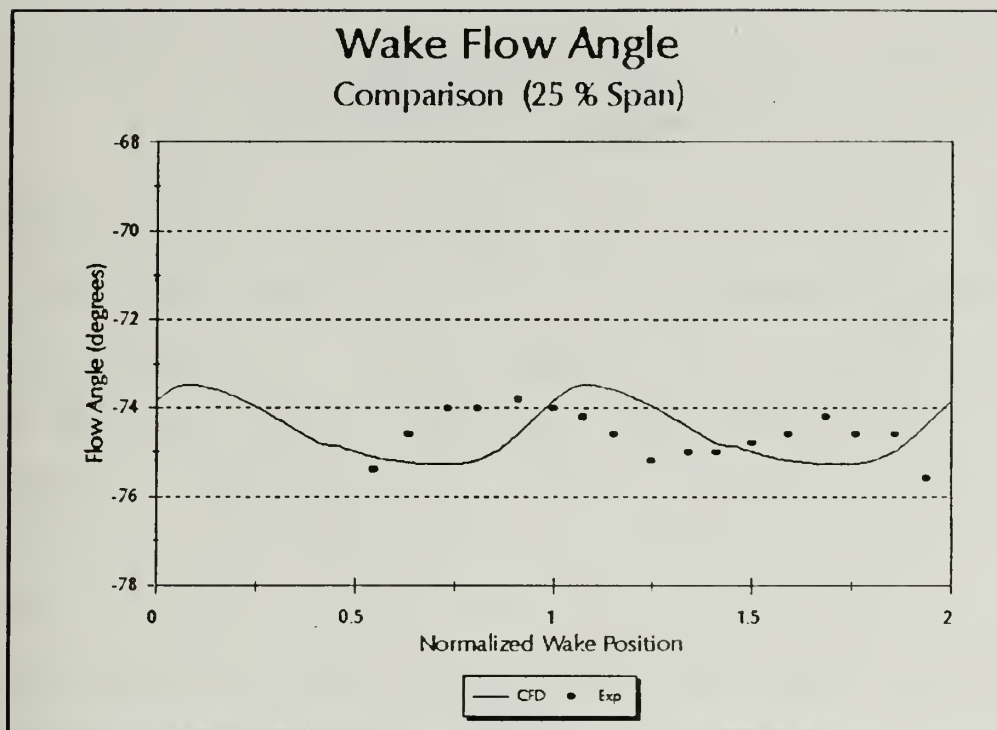


Figure 33. Flow Angle Comparison, 25%

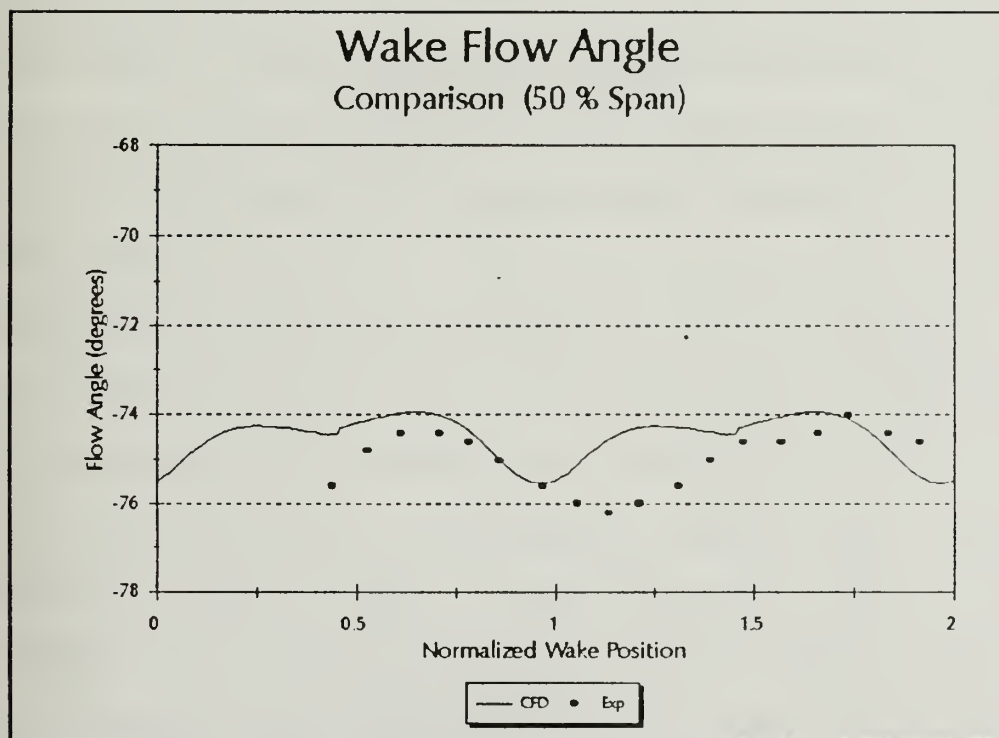


Figure 34. Flow Angle Comparison, 50%

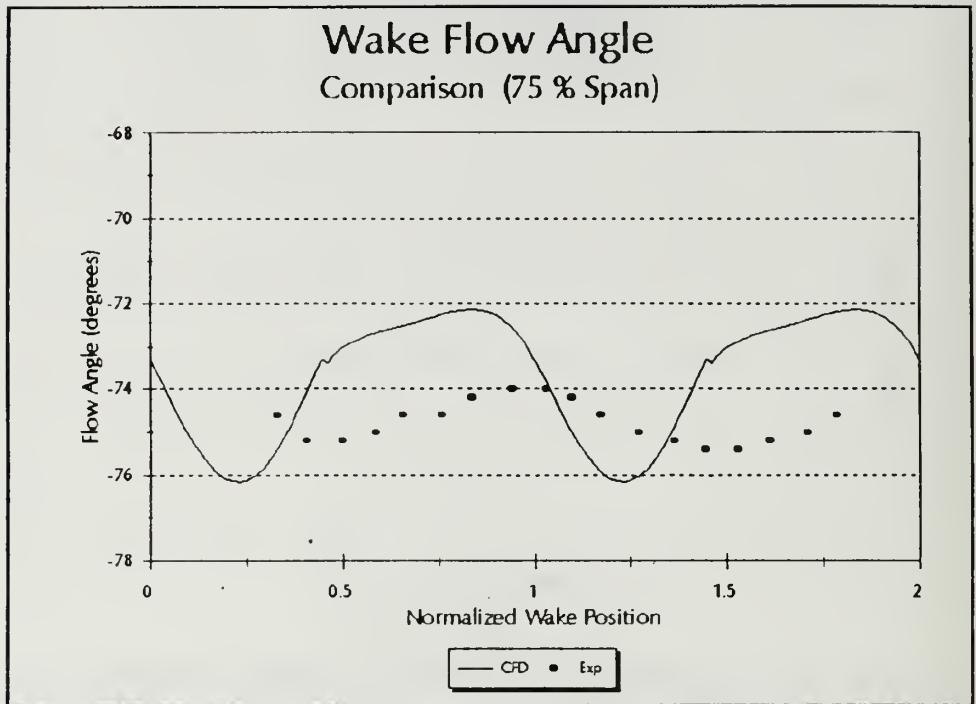


Figure 35. Flow Angle Comparison, 75%

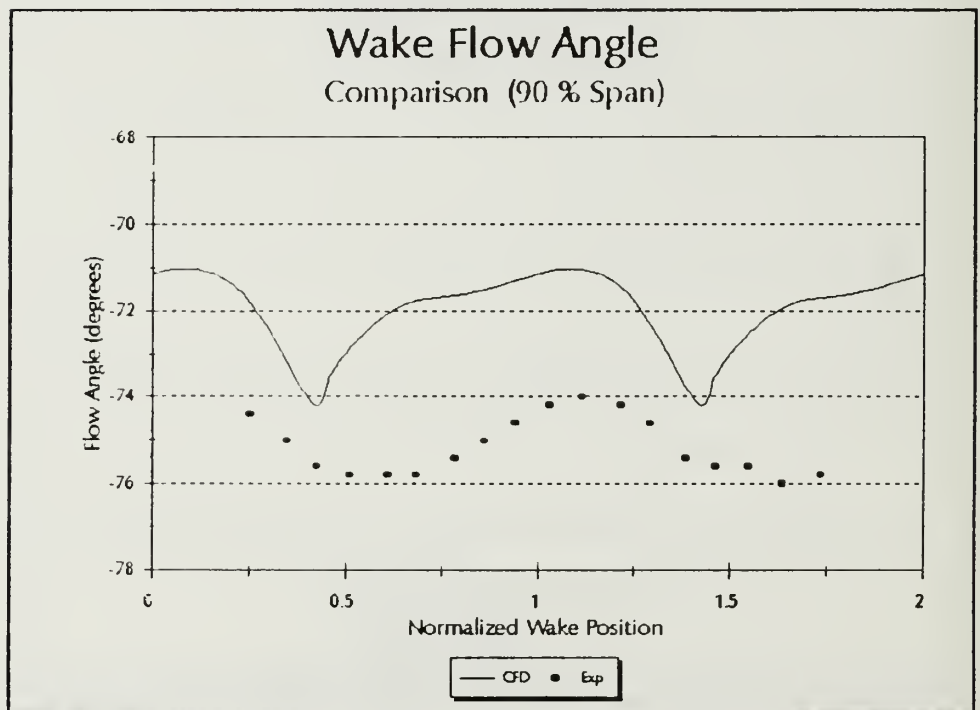


Figure 36. Flow Angle Comparison, 90%

V. CONCLUSIONS AND RECOMMENDATIONS

Experimental measurements and computational output locations were made to coincide. Repositioning the measurement volume to one-half axial chord downstream from the blade trailing edges improved the computational grid resolution. Flow solutions with the revised grid more realistically resolved endwall boundary layer characteristics so that future endwall LDV measurements will have a corresponding computed solution with equivalent resolution.

Pressure probe surveys will continue to be important in comparing experiment with CFD prediction. The cobra probe calibration obtained was reliable and repeatable. An extensive set of baseline data has been accumulated for future use. The Scanivalve data acquisition system demonstrated the ability to obtain pressure readings with a standard deviation of less than 0.2 percent. The HP-9000 output was manually entered into a spreadsheet program for post processing. The time required to manually enter the output was overshadowed by the spreadsheet data manipulation flexibility.

The most definitive comparison between CFD and probe measurements was in the total pressure ratio. Probe calibration error was not present in this comparison. The total pressure ratio disagreed by ten percent at the 25 percent spar location and less than one percent at the 90

percent location. In all cases, the computer solution predicted a lower ratio. The difference may be attributed to computational modeling parameters or bias introduced in the experimental pressure ratio setting. Upstream total pressure was measured at only one station and this value may not have been a proper reflection of the average total pressure. Mach number comparison characteristics followed the trend of the total pressure ratio as expected. Flow angle comparison with CFD was best at 25 percent span with a maximum difference of 5° at the 90 percent span location. Of all the measurement locations, the 90 percent span location was the best defined and flow angle measurements made there were repeatable within 0.2 degrees.

Endwall LDV through a small (1.0922 mm) casing access hole has been demonstrated. The ability to resolve endwall boundary layers and eventually tip flow losses appears to be promising. Precise LDV probe-volume positioning techniques were not obtained. The maximum pressure ratio attained for endwall LDV was 0.974. CFD and pressure probe data were accumulated at an operating pressure ratio of 0.68. Low data rate, vibration of the endwall hole, and thermal expansion problems will have to be dealt with as the operating pressure ratio is decreased to 0.68.

Future efforts with the computational fluid dynamics should include modeling the inlet bellmouth and center body. The parameters selected for use in RVC3D should also be

explored to obtain a qualitative feel for cause and effect on the solution with particular attention to the unsteady region of the exit flow.

Pressure data acquisition can be continued to obtain a more complete map of the wake region. Pressure instrumentation of a blade and passage would provide an additional source of CFD code validation data. Data reduction and presentation would be improved with a change in operating system. The current Scanivalve system with the HP-9000 does not allow file transfer to other computers for post processing. HP-9000 limitations restrict output flexibility.

The annular turbine cascade now has off-angle LDV options that have not been explored. Three-dimensional radial LDV surveys of the wake passage should be attempted for comparison with pressure measurements already obtained. Initial indications show that the LDV probe-volume energy may not be able to provide return signals of sufficient intensity as the flow velocity increases. The addition of corrective optics to the fiber-optic probe may be required.

The endwall technique developed in this study did not provide pressure equalization across the access hole. The pressure across the access hole should eventually be equalized to eliminate flow through the hole and therefore any influence the opening might have on the flow structure [Ref. 9]. The hole acted as a natural optical noise filter and further investigation of hole diameter influence on LDV performance is

warranted. In order to truly understand the hole influence and measurement reliability, the glycerin seed particle distribution and a study of their momentum characteristics should be undertaken. With these refinements, access to the flow through a hole in the casing is feasible, without changing the endwall flow characteristics.

APPENDIX A. DRAWINGS

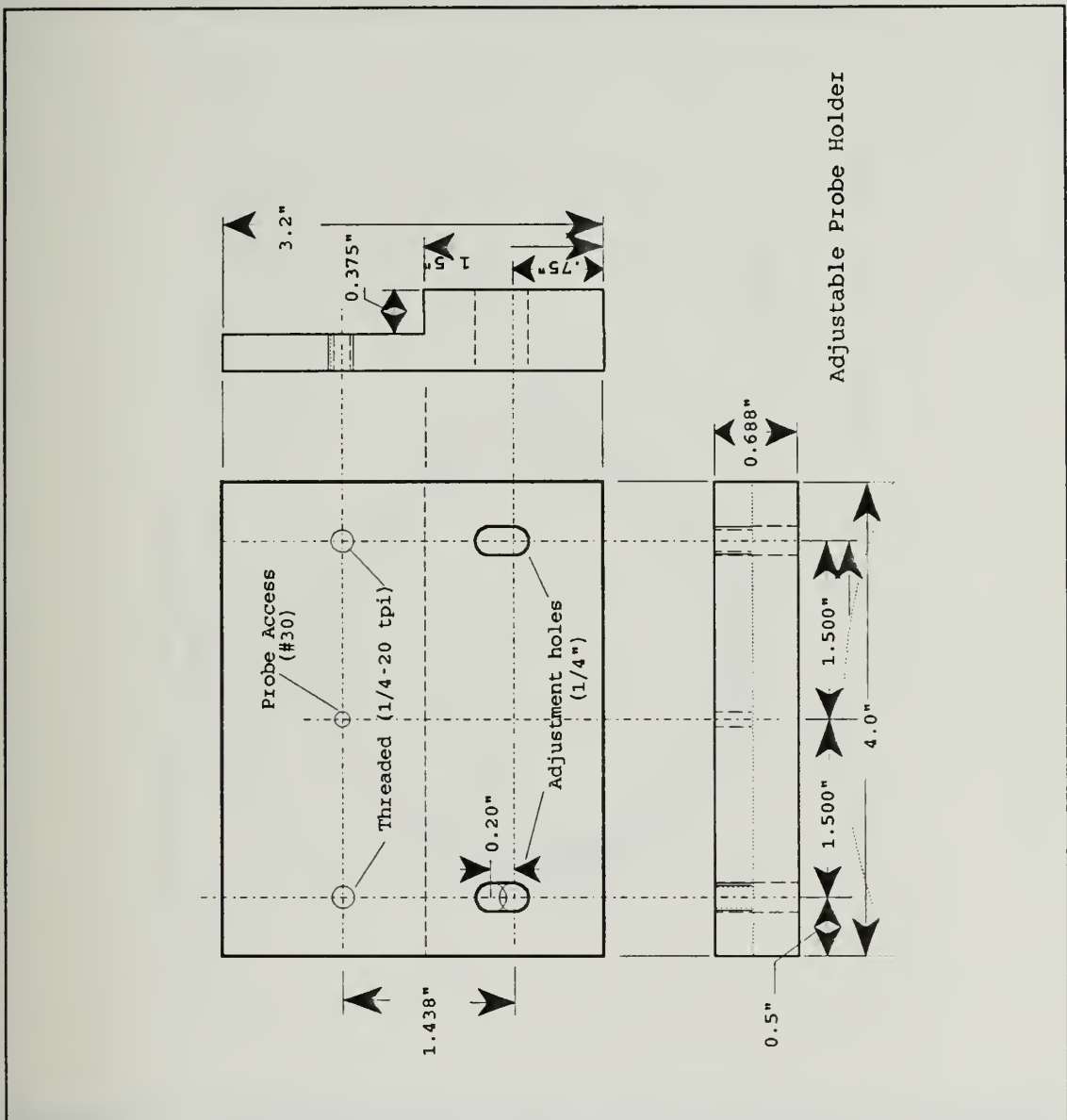


Figure A1. Adjustable Pressure Probe Holder

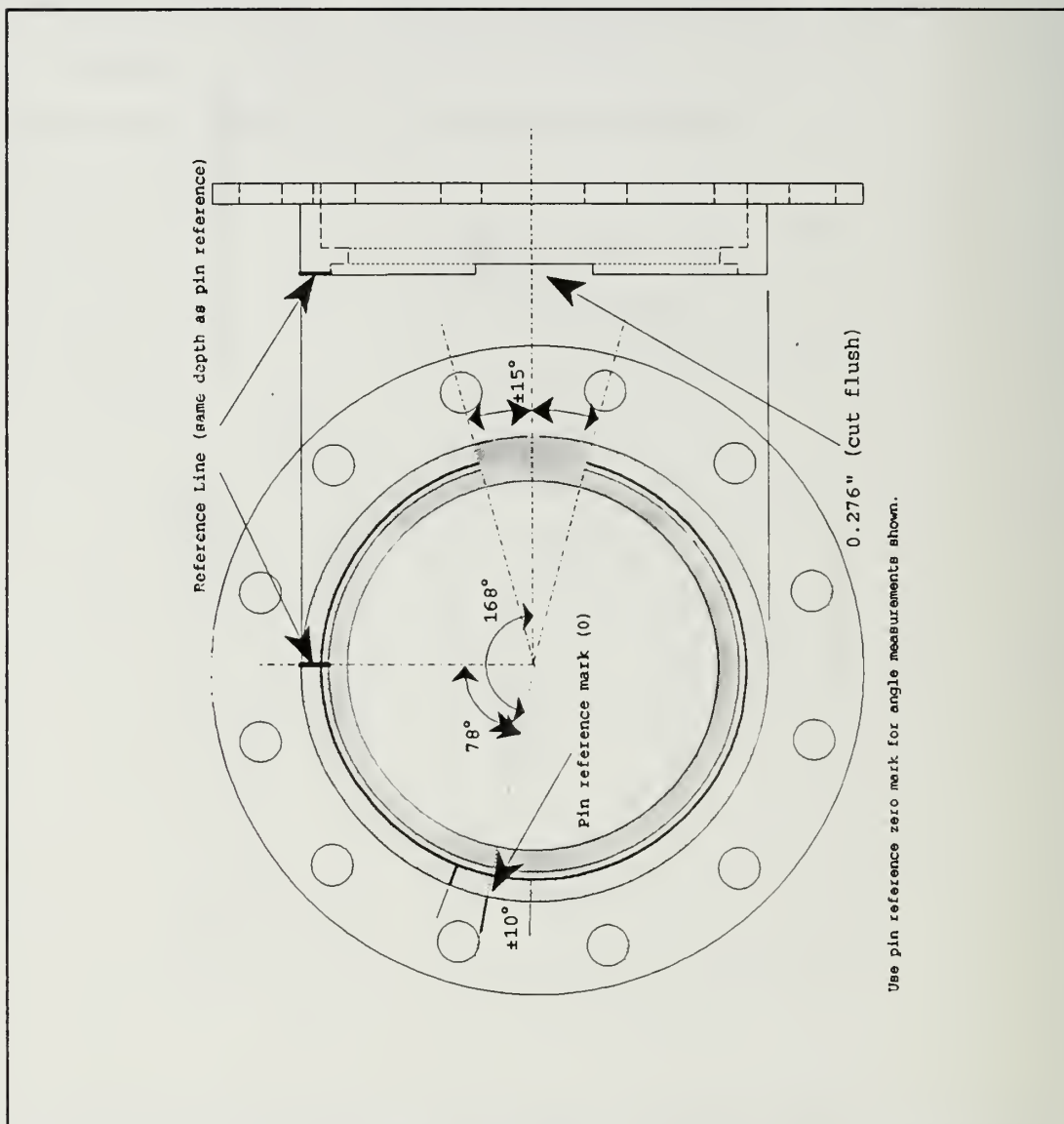


Figure A2. ATC Mounting Flange Modification

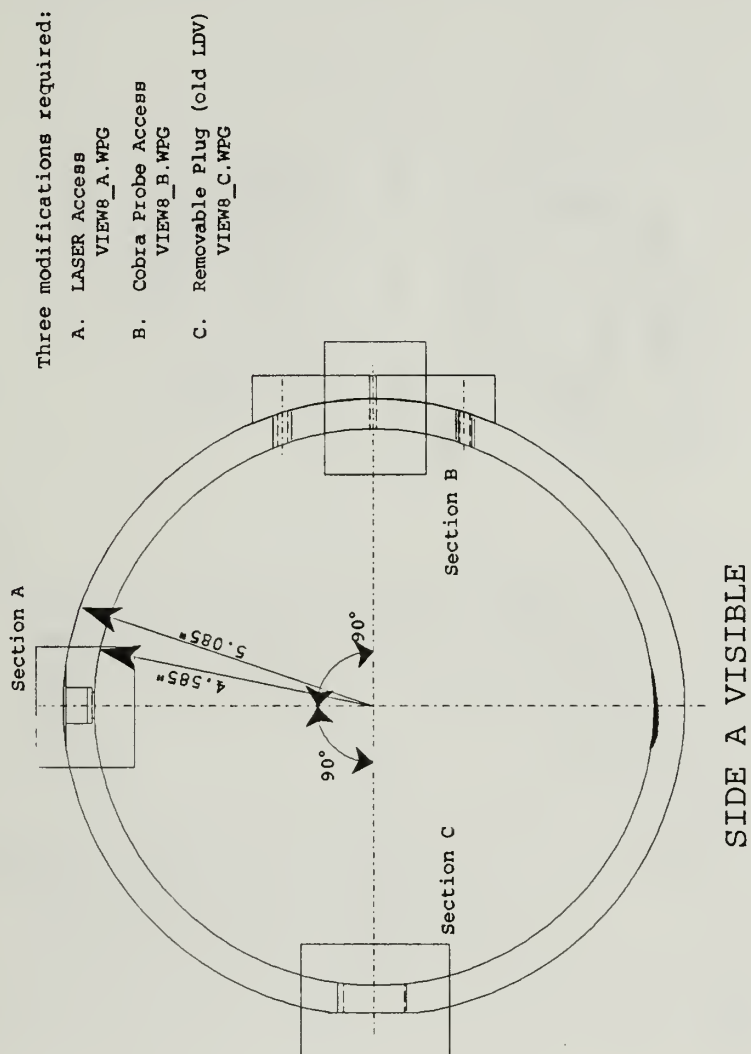


Figure A3. Outer Ring Modifications

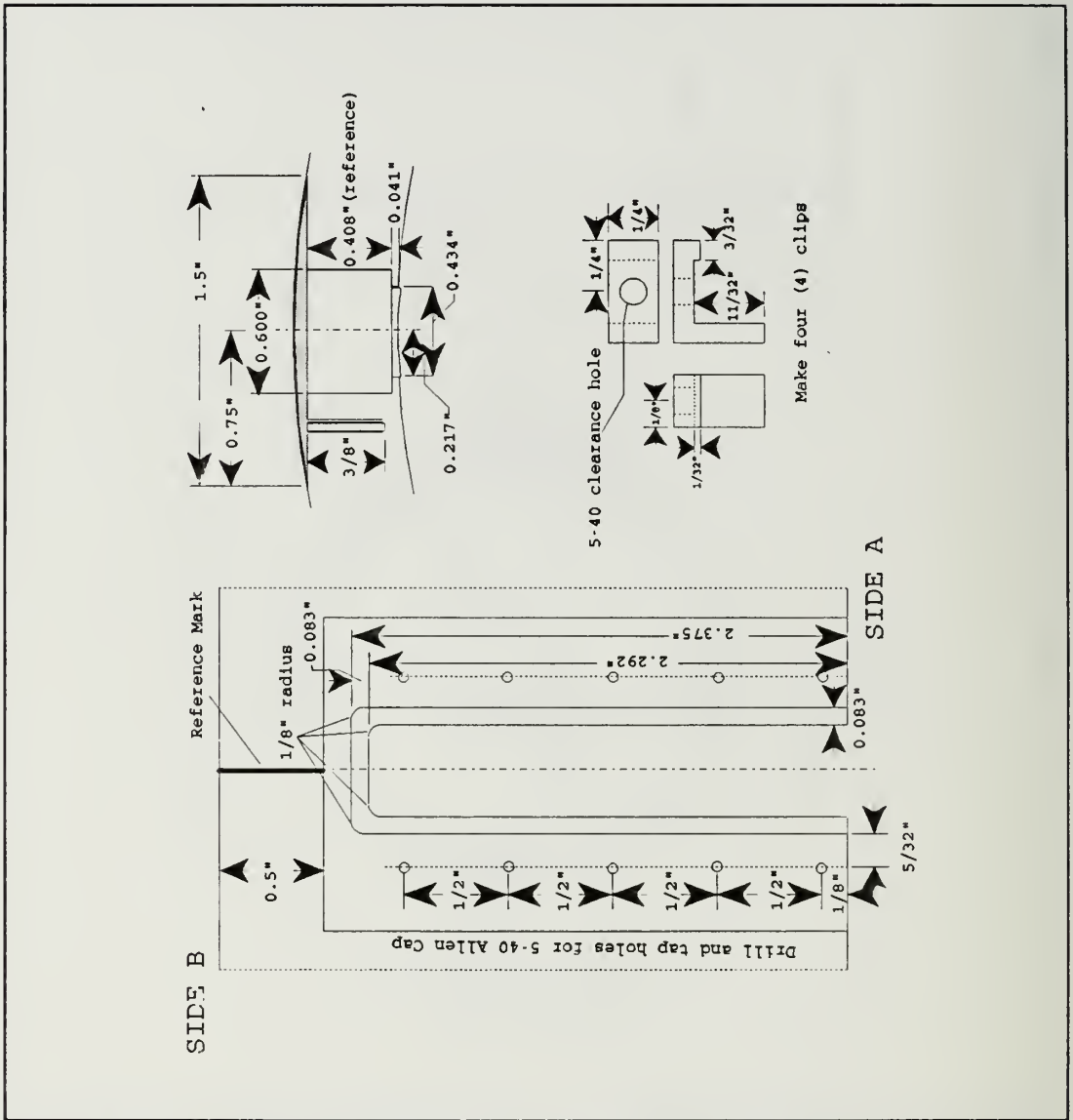
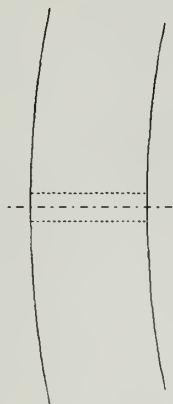
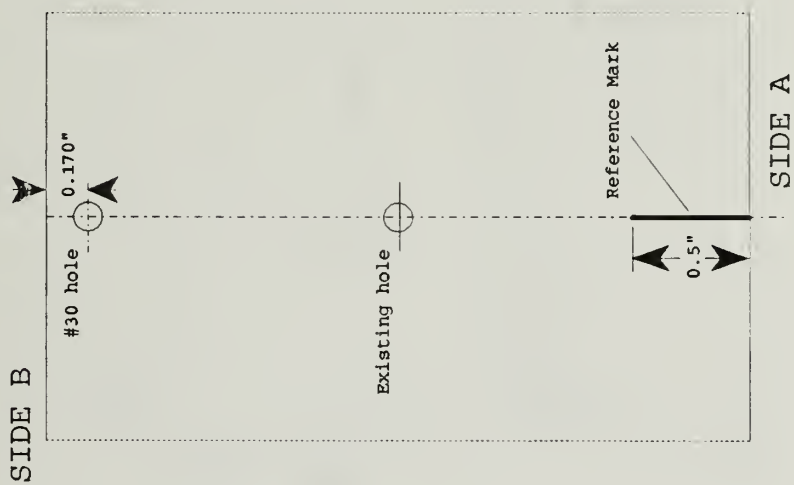


Figure A4. Outer Ring Modification, Section A



1. Reference Mark 90° from section A

Figure A5. Outer Ring Modification, Section B

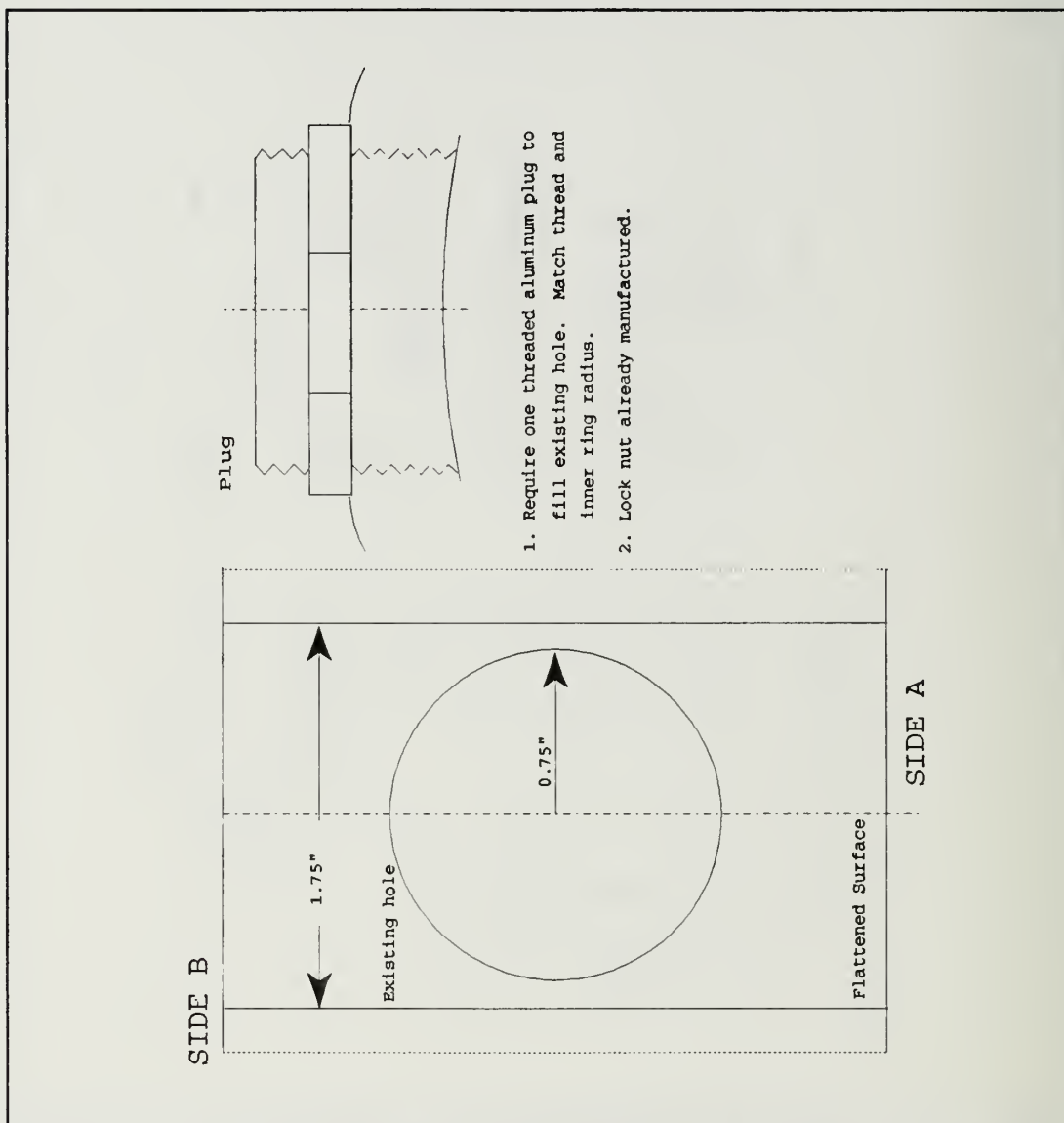
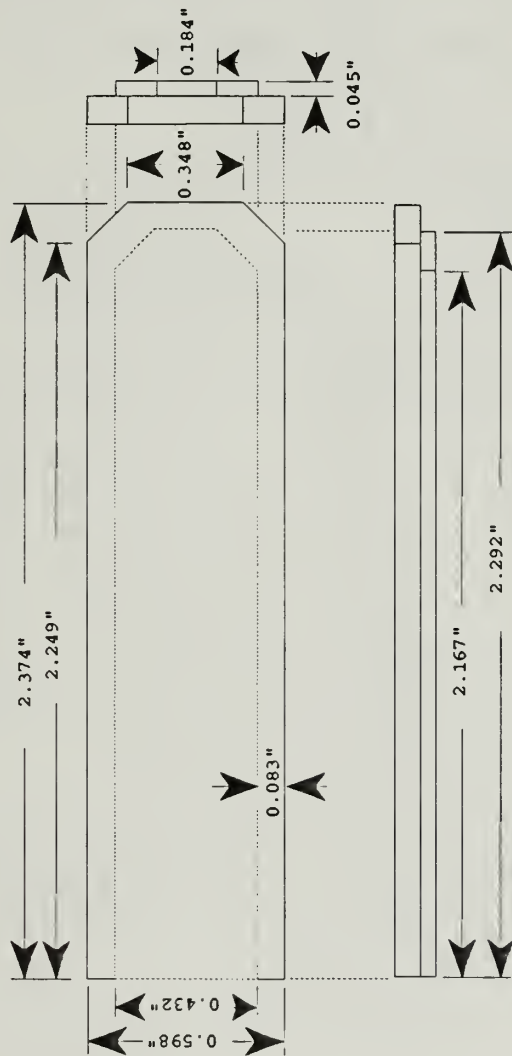


Figure A6. Outer Ring Modification, Section C



Material: 1/8" plexiglass

Quantity: 3 (three)

Figure A7. Plexiglas Window

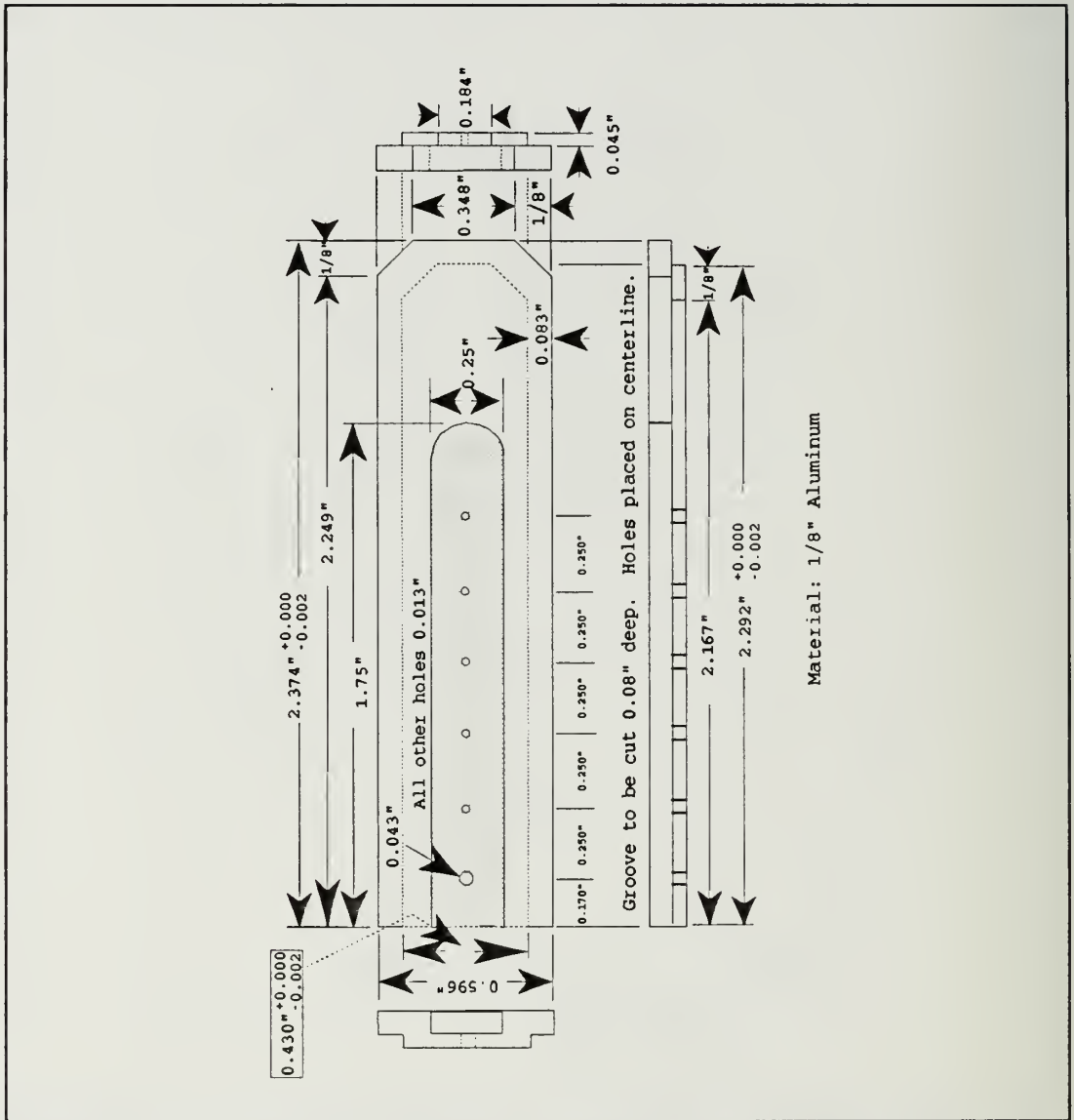


Figure A8. Alignment and Endwall Measurement Blank

APPENDIX B. COBRA PROBE CALIBRATION

The following synopsis was extracted from Appendix A of Reference 8. Mach number or dimensionless velocity can be related to a non-dimensional pressure coefficient, β , as follows:

$$\text{Total velocity:} \quad V_t = \sqrt{2C_p T_t}$$

$$\text{Dimensionless velocity:} \quad X = \frac{V}{V_t}$$

Dimensionless velocity and Mach number are related as follows:

$$\frac{C_p T_t - C_p T}{C_p T_t} = X^2$$

$$\frac{T}{T_t} = 1 - X^2$$

$$X = \frac{M \sqrt{\gamma R T}}{\sqrt{2 C_p T_t}}$$

so that

$$X^2 = \frac{\frac{\gamma-1}{2} M^2}{1 + \frac{\gamma-1}{2} M^2}$$

or

$$M^2 = \frac{2X^2}{(\gamma-1)(1-X^2)}$$

A pressure coefficient for the probe aligned in yaw can be written as

$$C_{p_{mn}} = \left(\frac{P_m - P_n}{P_m} \right) \left(\frac{P_m}{P_t} \right) \left(\frac{P_t}{P} \right) \left(\frac{2}{\gamma M^2} \right)$$

where p_m and p_n are probe sensor measurements. Using p_1 and p_{23} respectively, it can be shown that

$$\beta = \frac{P_1 - P_{23}}{P_1} = f(M, Pitch)$$

in the range of velocities which are of interest.

Figure C1 contains the calibration data without curve fitting and Figure C2 shows the validation data plotted against the sixth order and linear curve fits at zero pitch angle. The sixth order curve fit equation is

$$X = (a_0 + a_1\beta + a_2\beta^2 + a_3\beta^3 + a_4\beta^4 + a_5\beta^5 + a_6\beta^6) \times 100000$$

with the coefficients shown in Figure B1.

Pitch	a6	a5	a4	a3
-10	-6.660709305470791	3.544309861500551	-0.721451266749140	0.071316451905860
-8	-5.955775863135511	2.949084575351550	-0.572680326446530	0.055909732295640
-6	-4.637856128129431	2.538046396294830	-0.531511088605590	0.054545002333300
-4	-2.183311120542110	1.413296363564720	-0.336676175592050	0.038942145104620
-2	-6.274309176947050	3.100171008155951	-0.600635136590710	0.058315310608660
-1	-2.844367711631941	1.701006883697860	-0.391581825308930	0.044452699925970
0	-5.459055939566371	2.834115187282491	-0.574715603418510	0.057897300746720
1	-5.125554876288941	2.638195432256080	-0.529405283534050	0.052806276941470
2	-6.721219633789611	3.456184886424480	-0.688261827617630	0.067210456217870
4	-5.353574908692991	2.718292762333871	-0.539873695295450	0.053580419244550
6	-4.033033173685191	2.191961422867771	-0.463671350824480	0.048731080642020
8	-4.570212493067281	2.387287639075450	-0.485517019055070	0.049075329615750
	a2	a1	a0	
-10	-0.003592755586450	0.000105403602250	0.000000001566260	
-8	-0.002921288851680	0.000095660590210	0.000000001702560	
-6	-0.002910537590970	0.000094878475540	0.000000002131900	
-4	-0.002356713563080	0.000088606988900	0.000000000982640	
-2	-0.003006065023090	0.000095778340940	0.0000000001924690	
-1	-0.002619771949600	0.000092431757740	0.0000000002033150	
0	-0.003046971604010	0.000096483685640	0.0000000003581570	
1	-0.002779309853310	0.000091577051320	0.0000000000316970	
2	-0.003376285613260	0.000100227430950	0.0000000002122270	
4	-0.002823904337990	0.000092647421520	0.0000000002211020	
6	-0.002692393161270	0.000090870366840	0.0000000002330450	
8	-0.002621536570840	0.000087838669970	0.0000000001706990	

Figure B1. Cobra Probe Calibration Coefficients

Cobra Probe Calibration (Beta) Sensitivity to Pitch Angle

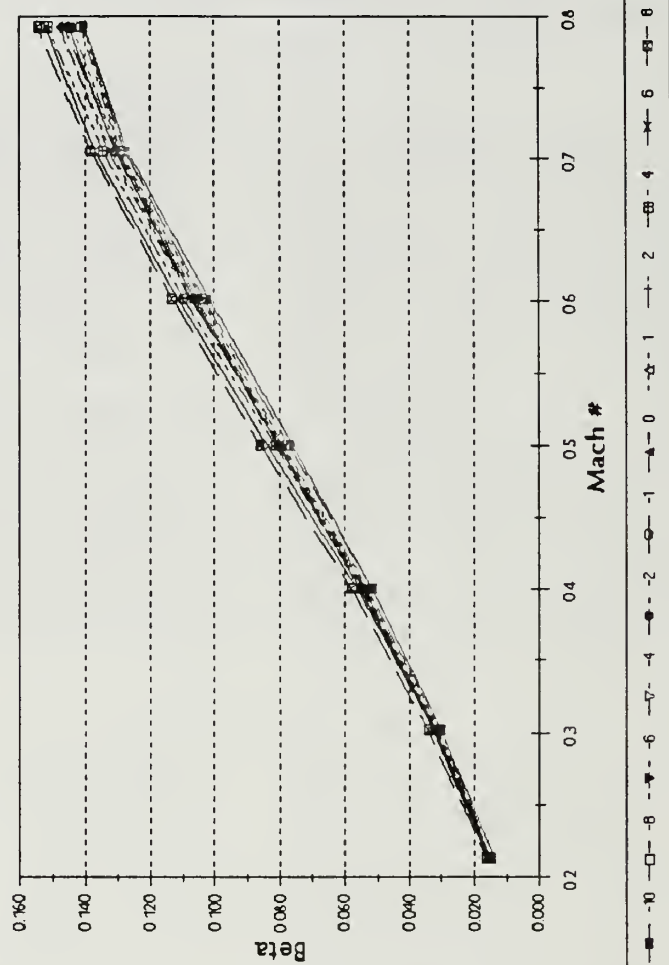


Figure B2. Cobra Probe Calibration Data Plot

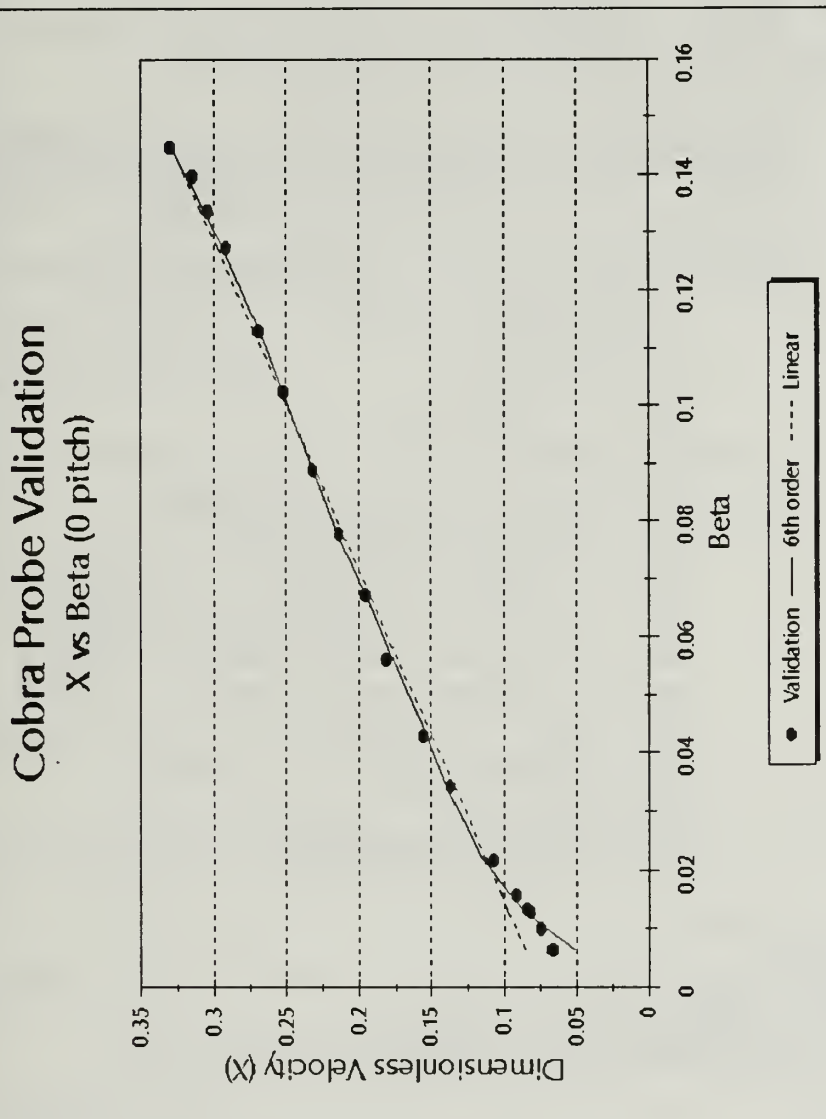


Figure B3. Probe Validation

Data acquisition was accomplished using an HP-9000 computer system with the following program:

```

10 !FILE NAME : COBRA_ATC
20 !DISK LABEL: "/AUSTIN"
30 ! LT JEFF AUSTIN
40 !LAST MODIFIED 02/03/94 BY LCDR JOE SPITZ
50 !
60 ! THIS PROGRAM RECORDS AND REDUCES MEASURED PRESSURES
70 ! FROM A Scanivalve CONNECTED TO A THREE HOLE PRESSURE
80 ! PROBE. Scanivalve PORT CONNECTIONS ARE AS FOLLOWS:
90 !
100 ! PROGRAM VARIABLES AND PORT CONNECTIONS...(#3 not used)
110 ! V = DESIRED S/V
120 ! A = PRESENT S/V PORT
140 ! C = CHANNEL
150 ! VO = DVM READING
160 ! S$ = SCANNER LISTEN CODE
170 ! S = SCANNER #
180 ! Scanivalve #5 SET TO ADVANCE ONLY
190 ! Pamb = Ambient Pressure (psi)
200 ! Patm = Atmospheric pressure...Port # 1
210 ! Pcal = Calibration pressure...Port # 2
220 ! Ptot = Reference total pressure...Port # 4
230 ! Phub = Inner hub static pressure...Port # 5
240 ! Pstat = Upstream static pressure...Port #6
250 ! P1 = Center hole on probe...Port # 7
260 ! P23 = Yaw port pressure...Port # 8
270 ! beta = (P1-P23)/P1
271 ! prar = Phub/Ptot (pressure ratio)
272 ! mach = mach(P1,Phub,Gamma)
280 !
290 OPTION BASE 1
300 Gamma=1.4
310 CLEAR SCREEN
311 PRINTER IS CRT
320 DISP "PLEASE WAIT WHILE RESETTING Scanivalves"
330 PRINT
340 V=5
350 A=1
360 GOSUB Read
370 !*****
380 PRINT "DATA ACQUISITION FOR THREE HOLE YAW PROBE"
390 DIM Y(20)
400 DIM Patm(10,10), Pcal(10,10),Ptot(10,10),Phub(10,10),Pstat(10,10)
410 DIM P1(10,10), P23(10,10)
420 !
430 INPUT "ENTER MONTH, DAY, YEAR (IE. 02,05,94)" ,Y(3), Y(5), Y(7)

```

```

431 INPUT "ENTER RUN #: ", Y(9)
432 PRINTER IS 711
440 PRINT USING "K,DD,""/""",DD,""/""",DD","DATE OF RUN:",Y(3),Y(5),Y(7)
441 PRINT "DATA RUN ",Y(9)
450 PRINT
451 PRINTER IS CRT
460 !*****
550 PRINT
560 PRINT "CONSTANT FLOW. WAKE: +9 TO -9 DEGREES. SPAN: 5 LOCATIONS
570 PRINT
571 PRINT " Zero DVM on Scanivalve #5, port #1."
572 PRINT
580 PRINT " Set 20 inHg for Scanivalve calibration."
581 PRINT
582 PRINT" Adjust span for DVM = 0.009823 volts on port #2."
600 PRINT
610 PRINT" ENSURE DVM ADJUSTED AND DESIRED PRESSURE RATIO SET..."
630 FOR WAKE = 1 TO 10
640 INPUT "ENTER AMBIENT PRESSURE IN inHg",Pinhg
641 Pamb=Pinhg*(.4911541)
650 PRINT
660 PRINT "CHECK DESIRED SPAN AND FLOW ALIGNMENT SET..."
661 PRINT
662 PRINT "*****PRESS CONTINUE WHEN READY TO TAKE DATA*****"
670 PAUSE
671 CLEAR SCREEN
680 PRINT
700 FOR SPAN = 1 TO 10
710 V=5
720 A=1
730 GOSUB Read
740 !*****
750 !
840 !*****
850 !RECORD THE PRESSURE DATA FOR THIS WAKE AND SPAN
860 !
870 !
880 OUTPUT 722;"F1R1T1M0Z1 " ! SETS UP HP3456A DVM
890 V=5 ! Scanivalve #5 DESIGNATED
900 S=1 ! HP3495A SCANNER #1 DESIGNATED
910 !
912 PRINTER IS 711
913 PRINT
914 PRINT "Wake Data Group ", WAKE
915 PRINT "Span Location Counter ", SPAN
916 PRINT USING "/",5X,K,DDD,/,2X,K,15X,K,17X,K";"
Scanivalve #",V,"Port","Volts","Psi"
919 PRINT
920 PRINTER IS CRT
921 !
922 ! READ Scanivalve PORTS

```



```

923 !
930     FOR A=1 TO 8
940         GOSUB Read
950         WAIT 2.0
960         OUTPUT 701;"C"                ! CLEARS SCANNER #1
970         OUTPUT 701 USING "DDD";V+9    ! SCANNER SET TO READ Scanivalve
                                           PORT
980         TRIGGER 722
990         ENTER 722;V0
1000        !*****
1002            PRINTER IS 711
1010        !   Pressure in psi
1020            IF A=1 THEN
1021                Patm(WAKE,SPAN)=V0*1000
1022                PRINT USING "2X,DDD,7X,7DD.DDDDDDD,8X,7DD.DDDD";
                    P,V0,Patm(WAKE,SPAN)
1023                PRINTER IS CRT
1024                PRINT USING "2X,DDD,7X,7DD.DDDDDDD,8X,7DD.DDDD";
                    P,V0,Patm(WAKE,SPAN)
1025                PRINTER IS 711
1026                END IF
1027        !
1030            IF A=2 THEN
1031                Pcal(WAKE,SPAN)=V0*1000
1032                PRINT USING "2X,DDD,7X,7DD.DDDDDDD,8X,7DD.DDDD";
                    P,V0,Pcal(WAKE,SPAN)
1033                PRINTER IS CRT
1034                PRINT USING "2X,DDD,7X,7DD.DDDDDDD,8X,7DD.DDDD";
                    P,V0,Pcal(WAKE,SPAN)
1035                PRINTER IS 711
1036                END IF
1037        !
1040            IF A=4 THEN
1041                Ptot(WAKE,SPAN)=(V0*1000)-Patm(WAKE,SPAN)+Pamb
1042                PRINT USING "2X,DDD,7X,7DD.DDDDDDD,8X,7DD.DDDD";
                    P,V0,Ptot(WAKE,SPAN)
1043                PRINTER IS CRT
1044                PRINT USING "2X,DDD,7X,7DD.DDDDDDD,8X,7DD.DDDD";
                    P,V0,Ptot(WAKE,SPAN)
1045                PRINTER IS 711
1046                END IF
1047        !
1050            IF A=5 THEN
1051                Phub(WAKE,SPAN)=(V0*1000)-Patm(WAKE,SPAN)+Pamb
1052                PRINT USING "2X,DDD,7X,7DD.DDDDDDD,8X,7DD.DDDD";
                    P,V0,Phub(WAKE,SPAN)
1053                PRINTER IS CRT
1054                PRINT USING "2X,DDD,7X,7DD.DDDDDDD,8X,7DD.DDDD";
                    P,V0,Phub(WAKE,SPAN)
1055                PRINTER IS 711
1056                END IF

```



```

1057      !
1060      IF A=6 THEN
1061      Pstat(WAKE,SPAN)=(V0*1000)-Patm(WAKE,SPAN)+Pamb
1062      PRINT USING "2X,DDD,7X,7DD.DDDDDDD,8X,7DD.DDDD";
          P,V0,Pstat(WAKE,SPAN)
1063      PRINTER IS CRT
1064      PRINT USING "2X,DDD,7X,7DD.DDDDDDD,8X,7DD.DDDD";
          P,V0,Pstat(WAKE,SPAN)
1065      PRINTER IS 711
1066      END IF
1067      !
1070      IF A=7 THEN
1071      P1(WAKE,SPAN)=(V0*1000)-Patm(WAKE,SPAN)+Pamb
1072      PRINT USING "2X,DDD,7X,7DD.DDDDDDD,8X,7DD.DDDD";
          P,V0,P1(WAKE,SPAN)
1073      PRINTER IS CRT
1074      PRINT USING "2X,DDD,7X,7DD.DDDDDDD,8X,7DD.DDDD";
          P,V0,P1(WAKE,SPAN)
1075      PRINTER IS 711
1076      END IF
1077      !
1080      IF A=8 THEN
1081      P23(WAKE,SPAN)=(V0*1000)-Patm(WAKE,SPAN)+Pamb
1082      PRINT USING "2X,DDD,7X,7DD.DDDDDDD,8X,7DD.DDDD";
          P,V0,P23(WAKE,SPAN)
1083      PRINTER IS CRT
1084      PRINT USING "2X,DDD,7X,7DD.DDDDDDD,8X,7DD.DDDD";
          P,V0,P23(WAKE,SPAN)
1085      PRINTER IS 711
1086      !
1087      prat=Phub(WAKE,SPAN)/Ptot(WAKE,SPAN)
1088      beta=(P1(WAKE,SPAN)-P23(WAKE,SPAN))/P1(WAKE,SPAN)
1089      mach=SQRT(5*(P1(WAKE,SPAN)/Phub(WAKE,SPAN))^(1/3.5)-5)
1090      END IF
1091      !
1092      NEXT A
1097      PRINT "prat = ", prat
1098      PRINT "beta = ", beta
1099      PRINT "mach # = ", mach
1100      PRINTER IS CRT
1101      PRINT
1102      PRINT "Set Span and align probe...CONTINUE WHEN READY..."
1103      PRINT
1104      PAUSE
1105      CLEAR SCREEN
1106      NEXT SPAN
1107      PRINT "Verify Wake & update Pamb...CONTINUE WHEN READY..."
1108      PRINT
1109      PAUSE
1110      CLEAR SCREEN
1111      NEXT WAKE

```

```

1112      !
1113      !*****END OF MAIN PROGRAM*****
1114      !
1115      !   SUBROUTINE TO POSITION AND READ S/V PORTS
1116      !           Scanivalve #1 HAS INOP HOME FEATURE
1117      Read:OUTPUT 707 USING '#,K';V
1118      PO=SPOLL(707)
1119      L=BINAND(PO,15)
1120      T1=ROTATE(PO,4)
1121      M1=BINAND(T1,7)
1122      P=10*M1+L
1123      CLEAR 707
1124      IF P=A THEN Finish
1125      OUTPUT 701; "C"
1126      OUTPUT 701 USING "DDD";V-1
1127      OUTPUT 701; "C"
1128      WAIT .1
1129      GOTO Read
1130      Finish:RETURN
1131      END

```

APPENDIX C. GRID GENERATION

Grid generation was completed on IRIS workstations. TCGRID, a FORTRAN program, required the adjustment of parameter statements to dimension arrays for the model build. Parameter adjustment required patience. The author found the manual helpful in most cases, however, the most useful tool turned out to be a running summary of the namelist input for troubleshooting. The most difficulty was observed in obtaining a smooth solution on the suction side of the blade geometry. The following TCGRID namelist file was utilized to obtain the grid shown in Figures C1 and C2. Reference 4 contains the original list of blade coordinates and is not included here.

```
&nam1 im=150 jm=31 km=65 itl=20 icap=18 k2d=3 merid=0 &end
&nam2 nle=16 nte=10 dsle=.018 dste=.003 dshub=.0004 dstip=.0004
      dswte=.001 dswex=.060 dsthr=1. dsmin=.0004 dsmax=.025
      dsra=.45 rcorn=.098 &end
&nam3 iterm=100 idbg=0 0 0 0 0 0 0 0 aabb=.5 codd=.45 &end
&nam4 zbc=-1.5 -1.5 0.5 -1.5 -1.5 .5
      rbc= 3.895 3.895 3.895 4.585 4.585 4.585 &end
```

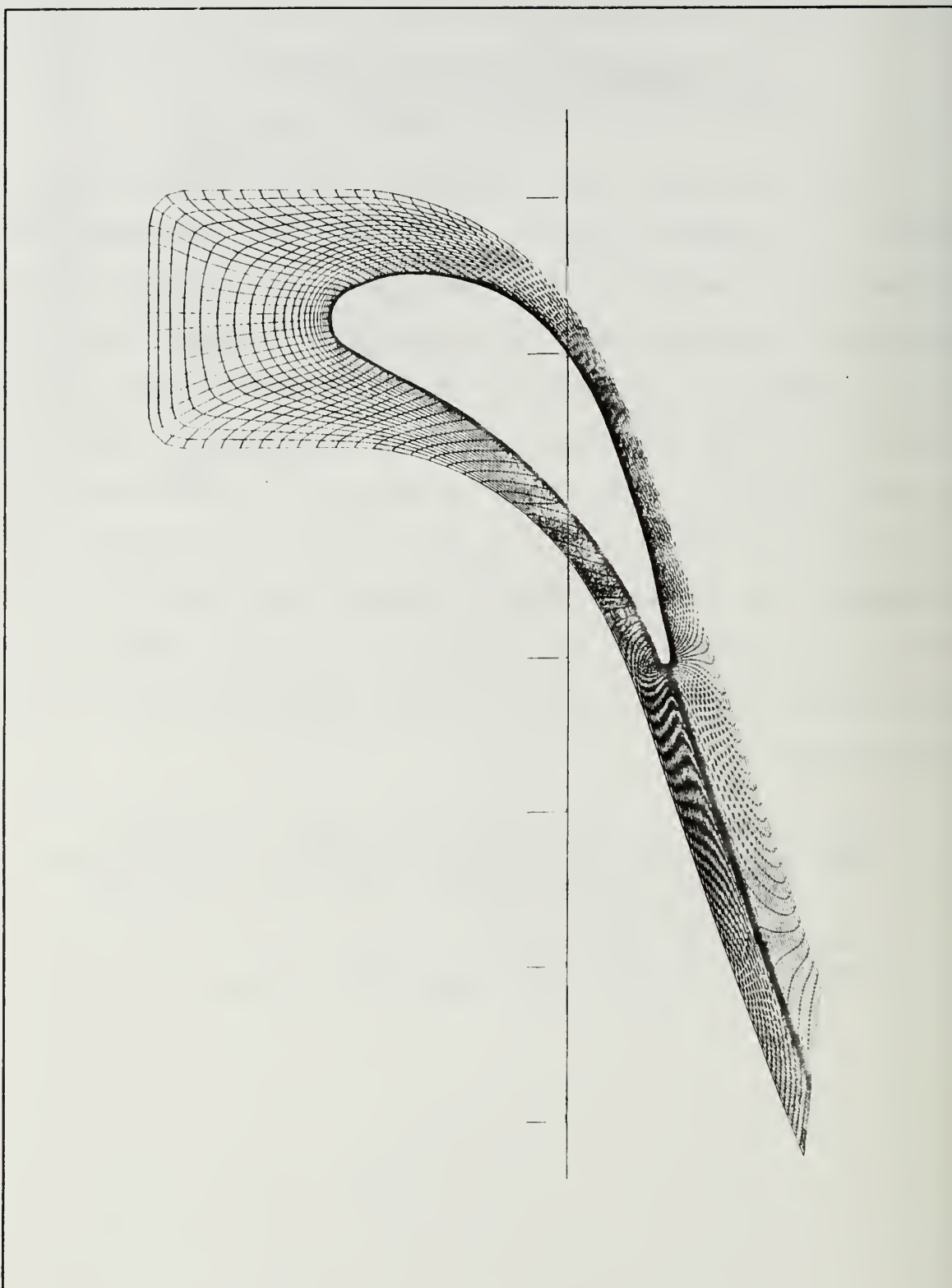


Figure C1. Grid Geometry On Inner Hub Surface

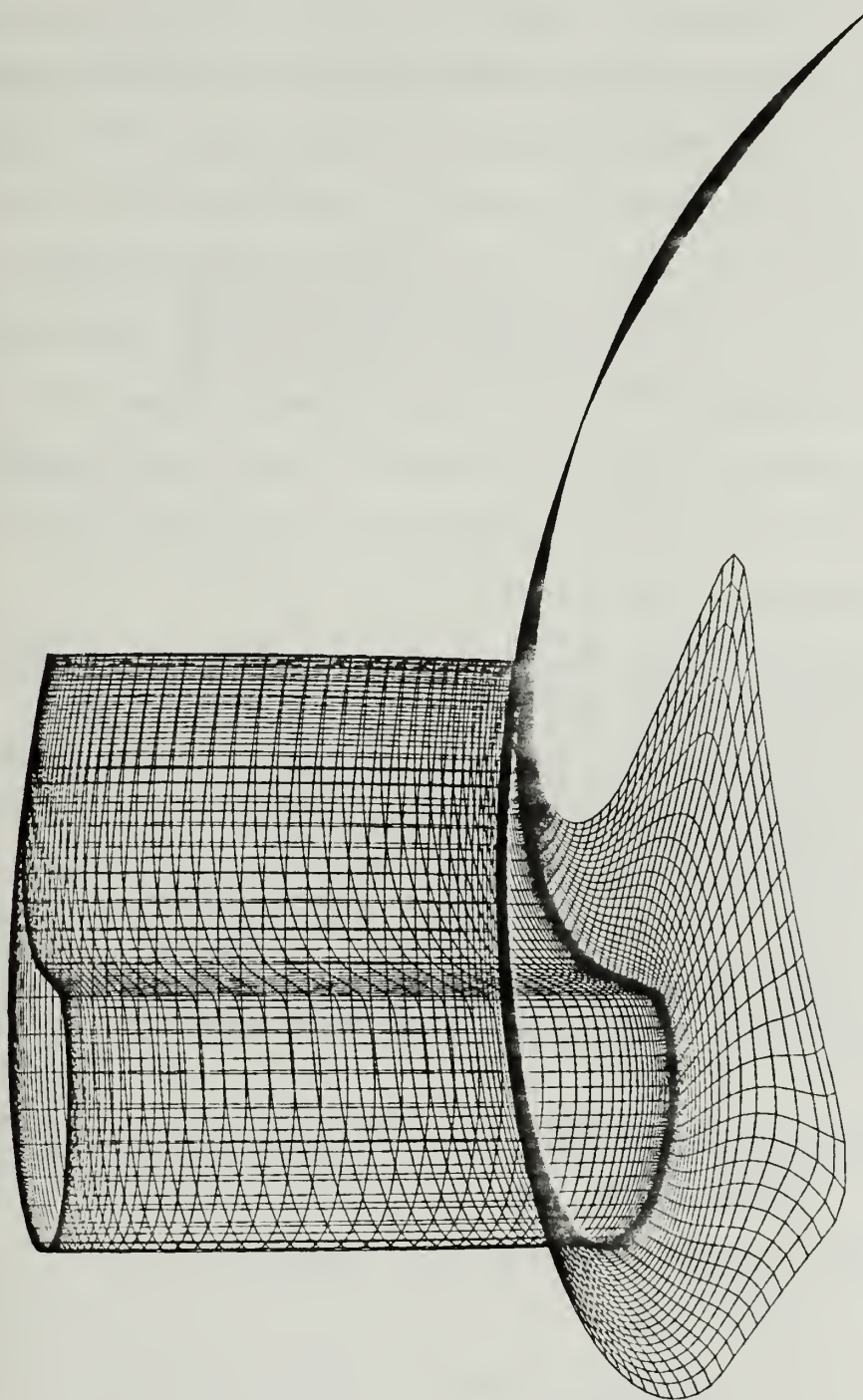


Figure C2. Grid Geometry, 3-D Perspective

APPENDIX D. RVC3D CODE INPUT

RVC3D runs were initially completed on IRIS workstations at NPS. Solutions were limited to less than 500 iterations to ensure residuals were decreasing. File transfer of the fort.1 (grid) and the rvc3d.in (namelist) files to the Cray were completed only after initial testing was completed. The following namelist contains the commands used for the final set of iterations to the minimum residual attainable. It is a restart (iresti=1) from 1200 iterations with termination at 1490 iterations (imax=290).

```
'TRANSONIC TURBINE Annular Cascade - (Restart 12-1490)'
&n11 im=150 jm=31 km=65 itl=20 iil=67 &end
&n12 cl=5.5 avisc1=0.0 avisc2=0.0 avisc4=0.50 ivdt=1
      nstg=4 itmax=290 irs=1 epi=0.50 epj=0.60 epk=0.60 &end
&n13 ibcin=3 ibcex=3 isymt=0 ires=10 icrnt=50
      iresti=1 iresto=1 ibcpw=0 iqin=0 &end
&n14 emxx=0.13 emty=0.0 emrz=0.0 expt=0.0 prat=0.6800
      ga=1.4 om=0.000000 igeom=1 alex=-67.0 &end
&n15 ilt=3 tw=1.00 renr=6.651e6 prmr=.7 prtr=.9
      vispwr=.666666 srtip=0.0 cmutm=14. jedge=31 kedge=20
      iltir=2 dblh=0.0024 dblt=0.0089 &end
&n16 io1=1 io2=165 oar=0. ixjb=0 njo=1 nko=3 jo=1
      ko=5 il 16 &end
```

Runs on the NPS cray were accomplished with the command

```
>qsub myjob.nqs
```

where the file myjob.nqs was as follows:

```
myjob.nqs
```

```
#QSUB -q reg -lT 43200 -lM 9Mw
cd cfd
rvc3d <rvc3d.in> rvc3d.out
```


The RVC3D executable, grid (fort.1), restart (fort.2), and the input namelist (rvc3d.in) were held in the subdirectory cfd. The final solution required 13.2 hours of Cray computer time. A plot of the residuals is shown in Figure D1.

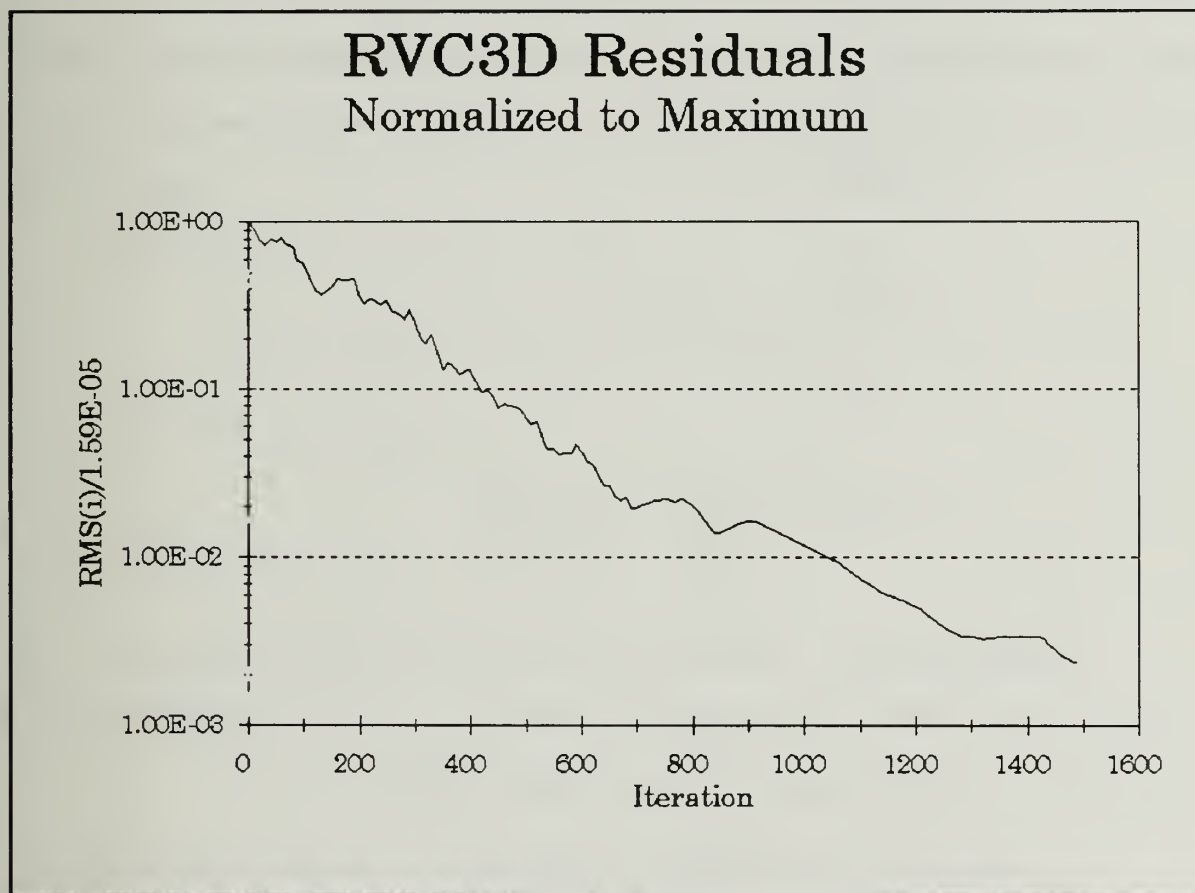


Figure D1. RVC3D Residuals

APPENDIX E. RVC3D DATA REDUCTION

Exit plane data were reduced using the FORTRAN program plane.f. RVC3D output the following non-dimensional values for each grid point in the file fort.3:

$$q_1 = \frac{\rho}{\rho_0}$$

$$q_2 = \frac{\rho u}{\rho_0 c_0}$$

$$q_3 = \frac{\rho v}{\rho_0 c_0}$$

$$q_4 = \frac{\rho w}{\rho_0 c_0}$$

$$q_5 = \frac{\rho}{\rho_0} \left[\frac{c_v T}{c_0^2} + \frac{1}{2} \left(\frac{u^2}{c_0^2} + \frac{v^2}{c_0^2} + \frac{w^2}{c_0^2} \right) \right]$$

Computational output was manipulated in plane.f for comparison with experimental results. The following table provides a coordinate system comparison.

Plot3d Cartesian	Annular Cascade	
	Cartesian	cylindrical
x(i) - u	z(i) - q2	z(i) - q2
y(i) - v	y(i) - q3	V _θ (i)
z(i) - w	x(i) - q4	V _r (i)

Transformation to cylindrical coordinates was conducted using the grid location information contained in the RVC3D grid input file fort.1.

$$\theta(i) = \sin^{-1} \left(\frac{y(i)}{\sqrt{y(i)^2 + z(i)^2}} \right) \quad r(i) = \sqrt{y(i)^2 + z(i)^2}$$

All angles (θ) were referenced to the y axis shown in the blade geometry plot of Figure 3. Flow angle computations were completed using the non-dimensional q values described above as follows:

Flow Angle Ψ (dimensional):

$$V_{\theta} = -(u) \sin \theta + (v) \cos \theta \quad V_r = (u) \cos \theta + (v) \sin \theta \quad V_z = w$$

$$\Psi = \tan^{-1} \left(\frac{V_{\theta}}{V_z} \right)$$

Flow Angle Ψ_{nd} :

$$V_{\theta_{nd}} = \frac{\rho V_{\theta}}{\rho_0 C_0} = -(q_4) \sin \theta + (q_3) \cos \theta \quad V_{z_{nd}} = \frac{\rho V_z}{\rho_0 C_0} = q_2$$

$$\Psi_{nd} = \tan^{-1} \left(\frac{V_{\theta_{nd}}}{V_{z_{nd}}} \right)$$

Direct comparison was possible with pressure ratio measurements. The ratio between local, and upstream reference total pressures was computed as follows:

$$\frac{P}{P_0} = \gamma (\gamma - 1) \left[q_5 - \frac{1}{2} \frac{\rho}{\rho_0} \left(\frac{u^2}{C_0^2} + \frac{v^2}{C_0^2} + \frac{w^2}{C_0^2} \right) \right]$$

$$\frac{p_t}{p_0} = \frac{p}{p_0} + \frac{1}{2p_0} \rho(u^2 + v^2 + w^2);$$

$$\frac{p_t}{p_0} = \gamma(\gamma-1) q_5 + \left(\gamma - \frac{\gamma^2}{2} \right) \frac{1}{q_1} (q_2^2 + q_3^2 + q_4^2)$$

Mach number was obtained using the isentropic relationship between Mach number and temperature ratio.

$$q_5 = \frac{q_1}{\gamma(\gamma-1)} \frac{T}{T_0} + \frac{1}{2q_1} (q_2^2 + q_3^2 + q_4^2)$$

$$\frac{T}{T_0} = \frac{\gamma(\gamma-1)}{q_1} \left[q_5 - \frac{1}{2q_1} (q_2^2 + q_3^2 + q_4^2) \right]$$

$$M = \sqrt{\left(\frac{T_0}{T} - 1 \right) \frac{2}{\gamma-1}}$$

The program plane.f is included here for reference. It is an updated version of the program written by Thomas [Ref. 4]. The new version includes a calculation of flow angles after conversion to cylindrical coordinates for proper comparison with experimental results.

```
C*****
C
C   plane.f reads rvc3d files & writes ascii files for plotting
C   exit plane mach number and flow angles
C   (comparison with experimental results)
C   unit 1 = input xyz file
C   unit 3 = input q file
C   unit 4 = output residual history
C   unit 7 = output (k #1) counter, theta, pt/p0, Mach, Angle
```

```

c      unit 8 = output (k #2) counter, theta, pt/p0, Mach, Angle
c      unit 9 = output (k #3) counter, theta, pt/p0, Mach, Angle
c      unit 10 = output (k #4) counter, theta, pt/p0, Mach, Angle
c      unit 11 = output (k #5) counter, theta, pt/p0, Mach, Angle
c
c*****
      parameter(ni=150,nj=31,nk=65)
      integer um
      real x(ni,nj,nk),y(ni,nj,nk),z(ni,nj,nk), gama
      real qq(5,ni,nj,nk,resd(5000,5),q1,q2,q3,q4,q5,m(5)
      dimension kk(5),ang(5),theta(5),tt0(5),vtnd(5),vrnd(5),
1  vznd(5),ptp0(5),deg(5)
c
c      k-values are hard-wired below (10%, 25%, 50%, 75%, 90%)
c      (use span.f to obtain %-k equivalency)
c
      data kk/21,27,33,39,45/
c*****
c      read grid coordinates
c*****
      read(1,*)im,jm,km
      read(1,*)((x(i,j,k),i=1,im),j=1,jm),k=1,km),
1      ((y(i,j,k),i=1,im),j=1,jm),k=1,km),
2      ((z(i,j,k),i=1,im),j=1,jm),k=1,km)
c*****
c      read restart file
c*****
      read(3,*)imax,jmax,kmax
      read(3,*)fsmach,alpha,re,time
c
      icheck=iabs(im-imax)+iabs(jm-jmax)+iabs(km-kmax)
      if(icheck.ne.0)then
      write(6,610) im,jm,km,imax,jmax,kmax
      stop
      endif
c
      read(3,*)((((qq(1,i,j,k),i=1,im),j=1,jm),k=1,km),l=1,5)
c
c      additional residual data
      read(3,*)itl,iil,phdeg,gama,om,nres,dum,dum,dum,dum
      read(3,*)((resd(nr,l),nr=1,nres),l=1,5)
c*****
c      Pressure side of exit wake cut...
c*****
      k=kk(3)
      i=1
      do 10 j=jmax,1,-1
      um=um+1
      do 15 l=1,5
      k=kk(l)
c

```

```

c   Rename desired q values for use
c
      q1=qq(1,i,j,k)
      q2=qq(2,i,j,k)
      q3=qq(3,i,j,k)
      q4=qq(4,i,j,k)
      q5=qq(5,i,j,k)
c
c   Compute pt/p0 ratio
c
      ptp0(1)=gama*(gama-1)*q5+(gama-gama**2/2)/q1*(q2**2+q3**2+q4**2)
c
c   Compute T/Tt ratio and mach number
c
      tt0(1)=gama*(gama-1)/q1*(q5-0.5*(q2**2+q3**2+q4**2)/q1)
      m(1)=(1/tt0(1)-1)**0.5/(gama-1)**0.5
c
c   Compute Theta and Non-D velocities theta, r and z
c
      theta(1)=asin(y(i,j,k)/(z(i,j,k)**2+y(i,j,k)**2)**0.5)
      vtnd(1)=-q4*sin(theta(1))+q3*cos(theta(1))
      vrnd(1)=q4*cos(theta(1))+q3*sin(theta(1))
      vznd(1)=q2
      deg(1)=theta(1)*57.296
c
c   Compute flow angle (degrees) using vtnd and vznd
c
      ang(1)=atan2(vtnd(1),vznd(1))*57.296
15  continue
      write(7,300)um,deg(1),ptp0(1),m(1),ang(1)
      write(8,300)um,deg(2),ptp0(2),m(2),ang(2)
      write(9,300)um,deg(3),ptp0(3),m(3),ang(3)
      write(10,300)um,deg(4),ptp0(4),m(4),ang(4)
      write(11,300)um,deg(5),ptp0(5),m(5),ang(5)
10  continue
c
c   Repeat above on other side of wake cut at imax
c   j=1 not used (duplicate location across wake)
c   jmax not repeated (same location as j=31 at i=1)
c
      jmaxm=jmax-1
      i=im
      do 30 j=2,jmaxm,1
        um=um+1
        do 25 l=1,5
          k=kk(l)
          q1=qq(1,i,j,k)
          q2=qq(2,i,j,k)
          q3=qq(3,i,j,k)
          q4=qq(4,i,j,k)
          q5=qq(5,i,j,k)

```



```

    ptp0(1)=gama*(gama-1)*q5+(gama-gama**2/2)/q1*(q2**2+q3**2+q4**2)
    tt0(1)=gama*(gama-1)/q1*(q5-0.5*(q2**2+q3**2+q4**2)/q1)
    m(1)=((1/tt0(1)-1)*2/(gama-1))**0.5
    theta(1)=asin(y(i,j,k)/(z(i,j,k)**2+y(i,j,k)**2)**0.5)
    vtnd(1)=-q4*sin(theta(1))+q3*cos(theta(1))
    vrnd(1)=q4*cos(theta(1))+q3*sin(theta(1))
    vznd(1)=q2
    deg(1)=theta(1)*57.296
    ang(1)=atan2(vtnd(1),vznd(1))*57.296
25  continue
    write(7,300)um,deg(1),ptp0(1),m(1),ang(1)
    write(8,300)um,deg(2),ptp0(2),m(2),ang(2)
    write(9,300)um,deg(3),ptp0(3),m(3),ang(3)
    write(10,300)um,deg(4),ptp0(4),m(4),ang(4)
    write(11,300)um,deg(5),ptp0(5),m(5),ang(5)
30  continue
C*****
c    residual history output to unit 4
C*****
    write(4,310) 1,(resd(1,1),l=1,5)
    do 40 j=2,nres
        it=10*(j-1)
    40 write(4,310) it,(resd(j,1),l=1,5)
C*****
300 format(i5,5f8.3)
310 format(i5,5(1x,e10.3))
610 format(' ***** warning *****',/,
1      ' im, jm, km, read from input',3i5,' do not match',/,
2      ' im, jm, km, read from restart file',3i5)
    stop
end

```


LIST OF REFERENCES

1. NASA Technical Paper 2018, "Laser Anemometer Measurements in an Annular Cascade of Core Turbine Vanes and Comparison With Theory," by Goldman, L. J., and Seasholtz, R. G., June 1982.
2. NASA Technical Paper 2846, "Three Component Laser Anemometer Measurements in an Annular Cascade of Core Turbine Vanes With Contoured End Wall," by Goldman, L. J., and Seasholtz, R. G., November 1988.
3. NASA Technical Paper 3252, "Laser Anemometer Measurements and Computations in an Annular Cascade of High Turning Core Turbine Vanes," by Goldman, L. J., and Seasholtz, R. G., July 1992.
4. Thomas, G. D., "Measurement and Prediction of the Flow Through an Annular Turbine Cascade", Master's Thesis, Naval Postgraduate School, Monterey, California, June 1993.
5. Dober, D. M., "Three-Dimensional Fiber-Optic LDV Measurements in the Endwall Region of a Linear Cascade of Controlled-Diffusion Stator Blades," Master's Thesis, Naval Postgraduate School, Monterey, California, March 1993.
6. Chima, Rodrick V., "TCGRID," program documentation prepared at NASA Lewis Research Center, November 1990.
7. Chima, Rodrick V., "RVC3D - Rotor Viscous Code 3-D," user's manual and documentation prepared at NASA Lewis Research Center, March 1992.
8. Neuhooff, F., "Calibration and Application of a Combination Temperature-Pneumatic Probe for Velocity and Rotor Loss Distribution Measurements in a Compressor," Contractor Report, Naval Postgraduate School, Monterey, California, pp. 44-49, December 1981.
9. Emanuel, G., "Gasdynamics: Theory and Applications," pp. 329-344, American Institute of Aeronautics and Astronautics, Inc., 1986.

INITIAL DISTRIBUTION LIST

	No. Copies
1. Defense Technical Information Center Cameron Station Alexandria VA 22304-6145	2
2. Library, Code 052 Naval Postgraduate School Monterey CA 93943-5002	2
3. Department Chairman, AA Department of Aeronautics and Astronautics Naval Postgraduate School Monterey CA 93943	1
4. Garth V. Hobson, Turbopropulsion Laboratory Code AA/Hg Department of Aeronautics and Astronautics Naval Postgraduate School Monterey CA 93940	10
5. Naval Air Systems Command AIR-536T (Attn: Mr. Mario Duffles) Washington DC 20361-5360	1
6. Naval Air Warfare Center Aircraft Division (Trenton) PE-31 (Attn: S. Clouser) 250 Phillips Blvd Trenton NJ 08628-0176	1
7. Joseph F. Spitz 517 E. Lake Rd. Box 178 Hammondsport NY 14840	2

DUDLEY FOX LIBRARY
NAVAL POSTGRADUATE SCHOOL
MONTEREY, CA 93943-5101

DUDLEY KNOX LIBRARY



3 2768 00307227 3